bioRxiv preprint doi: https://doi.org/10.1101/2025.01.16.632932; this version posted January 16, 2025. The copyright holder for this preprint (which was not certified by peer review) is the author/funder, who has granted bioRxiv a license to display the preprint in perpetuity. It is made available under aCC-BY-ND 4.0 International license.

1
2
3
4
5
6
7 **Multilayer regulation underlies the functional precision**
8 **and evolvability of the olfactory system**
9
10

11 Jérôme Mermet[1], Steeve Cruchet[1], Asfa Sabrin Borbora[1], Daehan Lee[1,#], Phing
12 Chian Chai[1], Andre Jang[2], Karen Menuz[2,3], Richard Benton[1,*]
13
14
15
16
17 [1]Center for Integrative Genomics
18 Faculty of Biology and Medicine
19 University of Lausanne
20 CH-1015
21 Lausanne
22 Switzerland
23
24 [2]Department of Physiology and Neurobiology
25 [3]Connecticut Institute for Brain and Cognitive Sciences
26 University of Connecticut
27 Storrs
28 Connecticut 06269
29 United States
30
31 [#]Present address:
32 Department of Biological Sciences
33 Sungkyunkwan University
34 Suwon 16419
35 Republic of Korea
36
37
38
39
40
41
42 [*]Corresponding author:
43 T: ++41 21 692 3932
44 E: Richard.Benton@unil.ch
45

bioRxiv preprint doi: https://doi.org/10.1101/2025.01.16.632932; this version posted January 16, 2025. The copyright holder for this preprint (which was not certified by peer review) is the author/funder, who has granted bioRxiv a license to display the preprint in perpetuity. It is made available under aCC-BY-ND 4.0 International license.

Abstract

Sensory neurons must be reproducibly specified to permit accurate neural representation of external signals but also able to change during evolution. We studied this paradox in the *Drosophila* olfactory system by establishing a single-cell transcriptomic atlas of all developing antennal sensory lineages, including latent neural populations that normally undergo programmed cell death (PCD). This atlas reveals that transcriptional control is robust, but imperfect, in defining selective sensory receptor expression. A second layer of precision is afforded by the intersection of expression of functionally-interacting receptor subunits. A third layer is defined by stereotyped PCD patterning, which masks promiscuous receptor expression in neurons fated to die and removes "empty" neurons lacking receptors. Like receptor choice, PCD is under lineage-specific transcriptional control; promiscuity in this regulation leads to previously-unappreciated heterogeneity in neuronal numbers. Thus functional precision in the mature olfactory system belies developmental noise that might facilitate the evolution of sensory pathways.

Introduction

Sensory systems mediate detection of the environment and provide the brain with a spatio-temporal code that enables recognition, interpretation and appropriate behavioral responses to a stimulus. However, the external world of stimuli changes as species colonize new ecological niches. Thus, sensory systems must also be capable of change over evolutionary timescales.

This paradox of functional precision but evolutionary flexibility is particularly notable in the olfactory system of *Drosophila melanogaster*. Intensive anatomical, molecular and functional analyses of the major olfactory organ, the third antennal segment (hereafter, antenna), have defined a highly stereotyped organization in which ~1200 neurons are categorized into nearly 50 distinct classes of olfactory sensory neurons (OSNs), as well as several types of hygrosensory and thermosensory neurons (Benton, 2022; Benton et al., 2025; Couto et al., 2005; Li et al., 2022; Li et al., 2020; McLaughlin et al., 2021; Schlegel et al., 2021; Vosshall and Stocker, 2007). Each class of olfactory neuron is characterized by the expression of a specific "tuning" receptor (belonging to the Odorant receptor (Or), Ionotropic receptor (Ir) or so-called "Gustatory" receptor (Gr) families), which defines chemical specificity, together with one or more broadly-expressed "co-receptors" (Orco for Ors; Ir8a, Ir25a, Ir76b for Irs). A few classes of neurons express more than one tuning receptor, typically encoded by tandemly-arranged gene duplicates. Antennal sensory neurons are grouped in combinations of 1-4 neurons underlying sensory hairs (sensilla) of several distinct morphological classes: antennal basiconic (ab), trichoid (at), intermediate (ai) and coeloconic (ac) (Figure 1A). The ciliated dendrites of OSNs are housed in the sensillar hair, while the axons project to the antennal lobe in the brain, where they innervate a glomerulus unique to each type of neuron.

The stereotypy is derived from apparently hard-wired developmental mechanisms. Each sensillum develops from a single sensory organ precursor (SOP) cell that is specified in the antennal imaginal disk in the larva (Figure 1A). The canonical view is that an SOP gives rise to a short, fixed lineage of asymmetric cell divisions that produces eight terminal cells with distinct molecular identity (Chai et al., 2019; Endo et al., 2007; Endo et al., 2011). Four of these eight cells become support cells (which have functions in sensillum construction and secretion of perireceptor

bioRxiv preprint doi: https://doi.org/10.1101/2025.01.16.632932; this version posted January 16, 2025. The copyright holder for this preprint (which was not certified by peer review) is the author/funder, who has granted bioRxiv a license to display the preprint in perpetuity. It is made available under aCC-BY-ND 4.0 International license.

96 proteins (Schmidt and Benton, 2020)), while the other four – termed Naa, Nab, Nba
97 or Nbb – can potentially give rise to OSNs (Chai et al., 2019; Endo et al., 2011).
98 Although two sensillum types do contain 4 OSNs, all other sensilla house fewer
99 neurons. This is thought to be due to programmed cell death (PCD) of precursor cells
100 during the pupal stage (Chai et al., 2019; Endo et al., 2007; Endo et al., 2011); in
101 many ac lineages the Nbb precursor is thought to differentiate as a glial cell (Endo et
102 al., 2007; Rodrigues and Hummel, 2008; Sen et al., 2005). Abundant evidence
103 supports the contribution of OSN-specific gene regulatory networks in defining the
104 fate of surviving neurons, notably in the precise transcriptional activation (or
105 inhibition) of receptor genes (Barish and Volkan, 2015; Jafari et al., 2012; Mika and
106 Benton, 2021; Mika et al., 2021). Such deterministic transcriptional codes are thought
107 to be central to the functional stereotypy of the olfactory system.

108 Comparison of the *D. melanogaster* olfactory system with other insects,
109 however, reveals remarkable evolvability, with changes in receptor function, receptor
110 expression and OSN number, often linked to adaptation of species to new ecological
111 niches (Hansson and Stensmyr, 2011; Ramdya and Benton, 2010; Zhao and
112 McBride, 2020). For example, in *Drosophila sechellia*, an extreme specialist on noni
113 fruit, olfactory channels detecting the host fruit exhibit altered receptor tuning and
114 expanded OSN populations (Auer et al., 2020; Prieto-Godino et al., 2017; Takagi et
115 al., 2024).

116 The generation of new receptors through tandem gene duplication and
117 functional diversification through sequence changes are conceptually straightforward
118 processes that are well-documented (Croset et al., 2010; Mika et al., 2021;
119 Robertson et al., 2003). By contrast, how novel cell types within a sensillum might
120 emerge is much less well-understood. One clue came from the demonstration that
121 blocking PCD is sufficient to result in the formation of functional OSNs (Prieto-Godino
122 et al., 2020), implying a latent potential of OSNs fated to die in evolving as new cell
123 types. Deeper understanding of this potential is precluded by our almost complete
124 lack of knowledge of how PCD is patterned in the developing OSN lineages, and the
125 molecular properties of individual neurons fated to die.

126 In this work, we generate a high-resolution, developmental atlas of the
127 antennal neuronal lineages, encompassing those that become functional neurons as
128 well as those that undergo PCD. We use this to define the first molecular
129 determinants specifying PCD of OSNs. Notably, we also discovered previously
130 overlooked heterogeneity in the patterning of receptor expression and PCD in the
131 olfactory system, which suggests how it might adapt during evolution.
132

133 **Results**

134

135 **Generation of an atlas of developing and dying antennal sensory neurons**

136

137 To generate a high-resolution, comprehensive, spatio-temporal atlas of the antennal
138 OSN lineages, we labelled these cells by using *pebbled-Gal4* (*peb-Gal4*), which is
139 expressed in all neural lineages (as well as many non-neuronal cells) from before 18
140 h after puparium formation (APF) (Sweeney et al., 2007), to drive a nuclear-GFP
141 reporter (*UAS-unc84:GFP*) (Henry et al., 2012). In parallel, to characterize the
142 developmental potential of neurons that are ultimately lost due to PCD during ~22-32
143 APF (Chai et al., 2019; Endo et al., 2007; Prieto-Godino et al., 2020; Sen et al.,
144 2004), we blocked OSN death by using *peb-Gal4* to also drive *UAS-p35*, encoding
145 the baculoviral P35 caspase inhibitor (Prieto-Godino et al., 2020). For both control

bioRxiv preprint doi: https://doi.org/10.1101/2025.01.16.632932; this version posted January 16, 2025. The copyright holder for this preprint (which was not certified by peer review) is the author/funder, who has granted bioRxiv a license to display the preprint in perpetuity. It is made available under aCC-BY-ND 4.0 International license.

146 and PCD-blocked genotypes, we dissected antennal tissues from animals sampled
147 every 6-8 h from 18-80 h APF, spanning the vast majority of their development
148 (Figure 1B). Antennae were pooled into "early" (18-30 h APF), "mid" (36-48 h APF)
149 and "late" (56-80 h APF) developmental stages prior to FACS isolation of GFP-
150 positive nuclei (Figure 1B). Using the 10X Genomics Chromium platform, we
151 sequenced the transcriptomes of ~54k and ~32k nuclei from control and PCD-
152 blocked antennae, respectively, detecting on average ~1000 genes/nucleus (Figure
153 S1A).
154 Unless mentioned otherwise (see Methods and legends), for all downstream
155 analyses we integrated control and PCD-blocked datasets, assuming that the vast
156 majority of cells would form equivalent clusters in these datasets, and that a smaller
157 number of "undead cells" would potentially form clusters unique to the PCD-blocked
158 dataset. To broadly catalog antennal cell types, we used marker genes extracted
159 from the Fly Cell Atlas (Li et al., 2022) (see Methods) (Figure S1B-C). Sensory
160 neurons – excluding Johnston's organ mechanosensory neurons – represent ~39%
161 of cells (~21,000) in the control dataset and ~43% (~14,000 cells) in the PCD-
162 blocked dataset (Figure S1D), consistent with the latter containing many undead
163 neurons (considered in more detail below). The remaining cells in our datasets
164 mostly represent sensillar support cells (Figure 1C and Figure S1D), suggesting that
165 *peb-Gal4* labels both neuronal and non-neuronal branches of the SOP lineages; the
166 latter cell types can be investigated in future studies.
167 We first annotated neurons within these datasets by developmental phase
168 (Figure 1D and Figure S2). All "branches" of cell clusters comprised a continuum
169 through early-, mid- and late-pupal stages (Figure 1D), each presumably reflecting
170 the development of different neuronal lineages. Each phase has distinct
171 transcriptional profiles (Figure S2): early-pupal stage neuronal markers were
172 enriched for genes involved in translation (likely reflecting enhanced protein synthesis
173 capacity); mid-pupal stage neuronal markers were enriched in genes involved in
174 signaling, cell-adhesion, axonogenesis and ion transport (concordant with the wiring
175 of antennal neurons in the brain (Jefferis and Hummel, 2006)); late-pupal stage
176 neurons expressed higher levels of genes involved in ion transport and synaptic
177 transmission (consistent with mature cell functions in neuronal signaling). Cells from
178 mid-developmental stages appeared to be the most transcriptionally divergent
179 between lineages, with late-stage neurons converging to a more similar gene
180 expression profile (as noted previously (McLaughlin et al., 2021)) (Figure 1D).
181
182 **High-resolution annotation of the developing antennal sensory neurons**
183
184 We subclustered these lineages at high resolution, annotating many clusters based
185 on the (chemo)sensory receptor gene(s) expressed in cells of the control dataset
186 (Figure S3). To annotate cells from earlier developmental stages – which mostly lack
187 expression of a diagnostic receptor gene – we used an iterative, retrograde
188 annotation method (see Methods). In brief, marker genes were extracted for each
189 individual neuron cluster – and/or groups of neurons housed in the same sensillum
190 ("sensillar markers") – and used to identify and annotate additional clusters. These
191 clusters were used as sources of additional earlier marker genes (see example
192 iterations in Figure S4). Ultimately, we could annotate ~90% of neurons (Figure 1E);
193 most of the remaining cells correspond to the earliest time points, which were difficult
194 to distinguish transcriptionally. A subset of these early cells expresses glial markers
195 (Figure 1E and Figure S3B); these might correspond to the Nbb-derived glia within

bioRxiv preprint doi: https://doi.org/10.1101/2025.01.16.632932; this version posted January 16, 2025. The copyright holder for this preprint (which was not certified by peer review) is the author/funder, who has granted bioRxiv a license to display the preprint in perpetuity. It is made available under aCC-BY-ND 4.0 International license.

196 the neuronal lineages (Endo et al., 2007; Rodrigues and Hummel, 2008; Sen et al.,
197 2005). The ~19,000 annotated neurons in our control atlas represent more than 15-
198 fold coverage of this sensory organ (~1200 neurons/antenna) (Grabe et al., 2016;
199 Schlegel et al., 2021).
200 Our annotation of sensory neurons allowed us to document the complements
201 of cell adhesion molecules, neurotransmitter receptors and ion channels for individual
202 neuron types (Figure S5), substantially extending previous analyses (McLaughlin et
203 al., 2021). Such information might point to additional molecules defining the specific
204 anatomical and functional properties of different sensory channels. In the context of
205 understanding the development of the olfactory system, we were also able to extract
206 markers for all sensillar classes (Figure 1F and Figure S6), and those distinguishing
207 the four neuron precursor types across essentially all lineages (Figure 1G and Figure
208 S7). The latter were enriched for genes encoding neural guidance molecules (Figure
209 S7C-D), concordant with the segregation of the OSNs from different precursor types
210 in the antennal lobe (Endo et al., 2007).
211 Our atlas encompasses all documented antennal sensory channels (Benton et
212 al., 2025). This contrasts with previous single cell/nuclear RNA-sequencing
213 (sc/snRNA-seq) analyses of the *D. melanogaster* developing antenna, which were
214 able to match only about one-third of known OSN types across three time points (24
215 h APF, 48 h APF and adult) (Li et al., 2020; McLaughlin et al., 2021) due to limited
216 cell numbers. To further assess the completeness of our dataset, we compared the
217 relative abundance of each sensory neuron class in the control dataset with those
218 expected by *in situ* analysis (typically using RNA FISH or sensory receptor promoter
219 reporter lines) (Benton et al., 2025). These values exhibited a remarkably strong
220 linear relationship, indicating the highly quantitative nature of cell representation in
221 our datasets (Figure 1H).
222
223 **Identifying transcription factors essential for lineage-specific development**
224
225 As a first assessment of the predictive ability of our developmental atlas and to
226 understand how precision in the olfactory map arises, we examined transcription
227 factors (TFs). Across pupal stages each neuronal population expresses a unique,
228 though often highly overlapping, combination of approximately 100 TF genes (Figure
229 S8). We tested the functional relevance of TF expression through study of three very
230 narrowly-expressed TF genes, which we reasoned might have selective and non-
231 redundant roles: *lozenge* (*lz*), encoding an AML/Runt family TF, which is expressed
232 exclusively in ab10 Or67a and Or85f neurons, and the tandemly-organized paralogs
233 *ladybird early* (*lbe*) and *ladybird late* (*lbl*), encoding NK-like homeobox TFs, which are
234 co-expressed in Or23a and Or83c neurons in ai2 (Figure 2A and Figure S8).
235 In all cases TF expression precedes that of the *Or* genes (Figure 2B-E). We
236 first validated these predicted expression patterns *in situ*, revealing selective
237 expression of the TFs in the expected neuron populations (Figure 2F and 2I). We
238 knocked down TF expression by using the *peb-Gal4* to drive TF RNAi transgenes
239 (Figure 2G-H and 2J-K). *lz*^{RNAi} led to essentially complete loss of expression of *Or67a*
240 and *Or85f*, while not affecting a control population expressing *Or67b*. *lbe*^{RNAi} had,
241 respectively, a mild or very strong effect on expression of *Or23a* and *Or83c*. While
242 *lbl*^{RNAi} alone barely affected expression of either receptor, it strongly enhanced the
243 *lbe*^{RNAi} phenotype, indicating partial redundancy of these TFs in ai2 neurons. This
244 function appears to be specific, as a control receptor Or43a was unaffected (Figure

bioRxiv preprint doi: https://doi.org/10.1101/2025.01.16.632932; this version posted January 16, 2025. The copyright holder for this preprint (which was not certified by peer review) is the author/funder, who has granted bioRxiv a license to display the preprint in perpetuity. It is made available under aCC-BY-ND 4.0 International license.

2K). Together, these data demonstrate an essential and selective role of *lz* and *lbe*/*lbl* in controlling ab10 and ai2 OSN development, respectively.

As *lz* and *lbe/lbl* are common to both OSNs within their respective sensilla, we hypothesize that these TFs act prior to the last lineage division that produces these distinct OSN types, rather than directly in receptor expression. Lbe/Lbl have previously been associated with cell fate specification in muscle and heart cells (Junion et al., 2007), rather than sensory neurons. By contrast, Lz was one of the first TFs implicated in antennal development, with a widespread role in antennal sensillar patterning that presumably occurs at an earlier stage within the antennal imaginal disc (Stocker et al., 1993). Our findings reveal a later, lineage-specific role for Lz, illustrating how TFs can play multiple roles within the development of this sensory system.

Precision and promiscuity of tuning receptor and co-receptor transcription

The analyses above indicate the comprehensive and functionally-predictive nature of our atlas, setting the stage for exploring how precision in the olfactory system is established. We first examined the spatio-temporal expression patterns of receptor genes (Figure 3A and Figure S9). In early developmental stages, only one gene was detected, the *Ir25a* co-receptor (discussed further below) (Figure S9). By mid-stages, transcripts for over a dozen tuning Irs or Ors in different populations of neurons, as well as *Ir8a* and *Ir93a* co-receptors, were detectable (Figure S9). By late stages, essentially all neuronal populations were reliably expressing a specific tuning receptor gene(s) (Figure 3A and Figure S9). As expected, the majority of these expressed a single tuning receptor, but our data confirmed the known cases of tuning receptor co-expression. The latter include the two subunits of the CO_2 receptor (*Gr21a/Gr63a*) (Jones et al., 2007; Kwon et al., 2007), cases of co-expression of genomically- and phylogenetically-distant receptor genes (e.g., *Or56a/Or33a*), and several examples of co-expression of closely-related, tandemly-arranged, receptor paralogs (e.g., *Or19a/Or19b*, *Or22a/Or22b*), where genes in these clusters likely retain conserved *cis*-regulatory sequences after gene duplication. We note that co-occurrence of *Ir75a*, *Ir75b* and *Ir75c* transcripts does not reflect co-expression of these genes, but rather runaway transcription in this cluster; protein-coding transcripts are expressed in distinct populations of OSNs (Mika et al., 2021; Prieto-Godino et al., 2017). While both Gr21a and Gr63a are essential for CO_2 responses (Jones et al., 2007; Kumar et al., 2020; Kwon et al., 2007), it is unclear whether the other cases of co-expression are functionally significant. Co-expressed paralogs might be functionally redundant or represent a transient evolutionary state as one paralog undergoes pseudogenization or neofunctionalization (Auer et al., 2022).

Our analyses revealed several cases of unexpected receptor expression. For example, *Or35a* is weakly expressed in ac4 Ir84a OSNs (Figure 3B), in addition to its well-described expression in ac3 neurons (Figure 3A). We confirmed these transcriptomic data *in situ*, detecting *Or35a* in ac4 sensilla, both in a subset of Ir84a neurons, as well as some Ir76a neurons (suggesting it was turned on in these cells at a later time point than we have profiled transcriptionally) (Figure 3C). Here, Or35a is unlikely to be functional, as Orco protein is not expressed in these neurons (Figure 3A); indeed, these neurons do not respond to ligands that activate Or35a neurons in ac3 (Silbering et al., 2011; Yao et al., 2005). We tested whether Or35a has the potential to be functional in Ir84a OSNs through transgenic expression of Orco in these cells, but this did not produce responses to Or35a-dependent ligands (Figure

bioRxiv preprint doi: https://doi.org/10.1101/2025.01.16.632932; this version posted January 16, 2025. The copyright holder for this preprint (which was not certified by peer review) is the author/funder, who has granted bioRxiv a license to display the preprint in perpetuity. It is made available under aCC-BY-ND 4.0 International license.

295 3D), suggesting that *Or35a* expression is too low, or that the transcript is aberrantly
296 spliced (Shang et al., 2024), and/or that other factors are required for Or35a function
297 (Figure 3E). *Or35a* transcripts were also detected in neurons of sacculus chamber III
298 (sacIII) (Figure 3A and Figure S10A-B), which correspond to the Amt-expressing
299 ammonia-sensing neurons (Vulpe et al., 2021); here it is also unlikely to be functional
300 as these cells do not express Orco (Figure 3A).
301 Another example of more promiscuous expression was observed for *Ir31a*,
302 which was detected in both Or47a and Or67d neurons, in addition to its own
303 population (Figure 3F). This expression is not detected *in situ* (Benton et al., 2009;
304 Silbering et al., 2011) and is unlikely to be functional as the essential Ir8a co-receptor
305 is not expressed in these neurons (Figure 3A), nor have they been described to
306 respond to Ir31a-dependent ligands (de Bruyne et al., 2001; Munch and Galizia,
307 2016; van der Goes van Naters and Carlson, 2007). Mis-expression of Ir8a in Or67d
308 neurons also failed to confirm sensitivity to the best known Ir31a agonist, 2-
309 oxopentanoic acid (Figure 3G). Closer examination of the transcriptomic data
310 revealed that *Ir31a* expression is transient, reaching highest levels prior to the branch
311 termini in these lineages; this pattern contrasts with *Or47a* and *Or67d* expression,
312 which peak at the end of the branches. We wondered whether this transient "ectopic"
313 expression of an *Ir* in these Or neurons reflected similarity in the gene regulatory
314 networks of these distinct cell types. Using information of differentially-expressed TFs
315 (Figure S8), we performed hierarchical clustering analysis of all OSN classes (Figure
316 3H). Notably, Ir31a, Or47a and Or67d neurons clustered within this tree, raising the
317 possibility that *Ir31a* "eavesdrops" on the complement of TFs of Or47a and Or67d
318 neurons to become transiently activated during development.
319 We extended our survey to receptors expressed in other chemosensory
320 organs (Figure S11). Amongst Ors, we detected transcripts of the maxillary palp
321 receptor *Or42a* in Ir31a neurons (Figure S11 and S10C). Again, this is unlikely to be
322 functional as Orco is not expressed in these cells (Figure 3A) (Benton et al., 2009),
323 and these neurons do not respond to Or42a ligands (Silbering et al., 2011). Several
324 *bona fide Gr*s were detected in a number of antennal cell types, consistent with
325 observations from previous transcriptomic and transgenic studies (Figure S11 and
326 S10D-E) (Fujii et al., 2015; McLaughlin et al., 2021; Menuz et al., 2014). The
327 functional significance, if any, of *Gr*s in the antenna in unclear (Pal Mahadevan et al.,
328 2022); we favor a hypothesis that such *Gr* expression merely reflects promiscuous
329 transcription of these genes, possibly due to overlap of the set of TFs present in
330 these antennal neurons and the gustatory neurons in which these receptors are
331 normally expressed.
332 Finally, our datasets confirm the previous observations of broad and partially
333 overlapping expression of various co-receptor genes (Figure 3A) (Abuin et al., 2011;
334 McLaughlin et al., 2021; Task et al., 2022). Whether co-receptors function in every
335 neuron in which they are expressed is unclear. Genetic and electrophysiological
336 analyses indicate an olfactory requirement for Ir8a only with selectively-expressed
337 acid-sensing tuning Irs (e.g., Ir31a, Ir64a), and Ir25a/Ir76b together only with amine-
338 sensing Irs (e.g., Ir41a, Ir76a) (Abuin et al., 2011; Vulpe and Menuz, 2021), despite
339 broader expression all three of these co-receptor genes (Figure 3A) (Abuin et al.,
340 2011; McLaughlin et al., 2021; Task et al., 2022). Loss of Ir25a has been described
341 to affect Or neuron sensitivity to stimuli, with mild increase or decrease of responses,
342 depending upon the neuron and the odor (Task et al., 2022), but the mechanistic
343 basis for such a variable effect on Or neuron responses is unclear. To our knowledge
344 there is only one case of a neuron (in ac3) that contains a functional complement of

bioRxiv preprint doi: https://doi.org/10.1101/2025.01.16.632932; this version posted January 16, 2025. The copyright holder for this preprint (which was not certified by peer review) is the author/funder, who has granted bioRxiv a license to display the preprint in perpetuity. It is made available under aCC-BY-ND 4.0 International license.

345 tuning and co-receptor Ors and Irs (Benton et al., 2025). We suggest that
346 contributions of broadly-expressed co-receptors is constrained by the selective
347 expression of partner tuning subunits: just as tuning receptors without co-receptors
348 are likely to be non-functional, co-receptors without partners might have no or
349 minimal sensory contributions.
350
351 **Heterogeneous life and death fates of specific OSN populations**
352
353 We next turned our attention to the neurons that are normally removed by PCD
354 during antennal development. While such cells can develop into functional sensory
355 neurons when PCD is blocked (Prieto-Godino et al., 2020), we know little about their
356 molecular and developmental properties. To identify cells in the atlas corresponding
357 to those that undergo PCD, we examined the expression of the pro-apoptotic genes
358 *reaper* (*rpr*), *grim*, *sickle* (*skl*) and *head involution defective* (*hid*) as one or more of
359 these genes are transcriptionally upregulated prior to PCD in many developmental
360 contexts (Pinto-Teixeira et al., 2016) (Figure 4A). Indeed, we detected higher
361 expression of *rpr*, *grim* and *skl* in the PCD-blocked dataset than the control dataset,
362 with largely overlapping expression patterns of these genes in a subset of cell
363 clusters representing putative undead neurons (Figure S12A-B). By contrast, *hid* was
364 expressed at similar levels in both PCD-blocked and control datasets (Figure S12A-
365 B), indicating that this gene is not a selective marker of cells that are fated to die (as
366 noted in other tissues (Pinto-Teixeira et al., 2016)), and was therefore discounted as
367 a marker. We therefore combined expression enrichment of *rpr*, *grim* and *skl* into a
368 single "RGS score", as a quantitative measure of the likelihood that a cell type was
369 fated to die (Figure 4B-C).
370 We next decomposed the atlas of integrated control and PCD-blocked
371 datasets (Figure 1E) into individual sensilla, using sensillar markers (Figure 1F and
372 Figure S6) and compared cells from each dataset. We reasoned that some undead
373 neurons might form cell clusters unique to the PCD-blocked dataset, as investigated
374 in the next section. However, as many undead neurons express receptors
375 characteristic of normal populations of OSNs (Prieto-Godino et al., 2020), we first
376 asked whether any such cells are embedded in clusters of these normal cells,
377 thereby simply creating a larger cluster in the PCD-blocked dataset. Given the highly
378 quantitative representation of cell populations in our antennal atlas (Figure 1H), to
379 identify such undead neurons, we first compared the relative proportion of each
380 neuronal type in control and PCD-blocked datasets (Figure S12C and Figure 4D).
381 While neurons housed in the same sensillum generally displayed similar
382 representations within and across datasets (e.g., Or56a/Or33a and Or7a neurons in
383 ab4, or Or67c and Or98a neurons in ab7, Figure 4D), in several cases in the control
384 dataset we observed different proportions of co-housed neurons. For example, in
385 ab10 Or85f neurons are underrepresented compared to Or67a neurons, and in the
386 trichoid sensillum at4 Or65a/b/c neurons are less abundant than Or47b and Or88a
387 neurons (Figure 4D). Importantly, these mis-matched neuronal representations were
388 at least partially re-equilibrated in the PCD-blocked atlas (Figure 4D and Figure
389 S12C), suggesting individual cell types within a subset of sensilla are
390 developmentally lost due to death.
391 Focusing first on ab10, we investigated this possibility initially by comparing
392 the pro-apoptotic gene RGS score within individual neuron lineages (Figure 4E). We
393 observed that the Or85f branch has a higher score, consistent with the occurrence of
394 PCD in a subset of these cells. In agreement with these transcriptomic data, RNA

bioRxiv preprint doi: https://doi.org/10.1101/2025.01.16.632932; this version posted January 16, 2025. The copyright holder for this preprint (which was not certified by peer review) is the author/funder, who has granted bioRxiv a license to display the preprint in perpetuity. It is made available under aCC-BY-ND 4.0 International license.

395 FISH for these receptor transcripts revealed a lower number of Or85f neurons
396 compared to Or67a neurons in the antenna; while all of the former are paired with the
397 latter, we detected several cases of isolated Or67a neurons in control animals, but
398 not when PCD was blocked (Figure 4F-G).
399 Next, we examined at4 (Figure 4H). Here, the underrepresented Or65a/b/c
400 neurons display a higher RGS score during their lineage development compared to
401 Or47b and Or88a lineages. *In situ*, we detected many fewer Or65a neurons than
402 Or47b and Or88a; while the latter two neuron types were always paired, only a
403 subset formed a triplet with Or65a neurons in control animals (Figure 4I-J). These
404 observations match those from electron microscopic studies describing the existence
405 of at4 sensilla housing only two neurons (Nava Gonzales et al., 2021). In PCD-
406 blocked antennae, only the number of Or65a neurons was increased – and all were
407 closely associated with Or47b and Or88a neurons – indicating a subset of these
408 neurons are also naturally removed by PCD (Figure 4I-J). While these *in situ* data
409 indicate 1:1:1 correspondence, we note that within the PCD-blocked dataset,
410 Or65a/b/c neurons were still underrepresented (Figure 4D), suggesting that this
411 dataset lacks annotation of some undead neurons (discussed further below).
412 Together these observations indicate that PCD acts within several sensilla
413 lineages to selectively remove a subfraction of OSNs normally considered to
414 represent a fully surviving lineage (as opposed to the lineages that are fated to die,
415 which we consider in the next section). It is surprising that such heterogeneity has not
416 been reported previously. In part this might reflect the relatively limited data co-
417 visualizing neurons within the same sensilla in whole-mount antennae – as opposed
418 to cryosections (e.g., (Couto et al., 2005)) – which is essential to view the pairing
419 patterns of the entire cell population. Additionally, it is possible that during
420 electrophysiological recordings, sensilla that do not have the "expected" numbers of
421 neurons are disregarded from detailed study. The functional significance of sensillum
422 heterogeneity is unclear. While the lack of specific neurons in sensilla would
423 eliminate the ephaptic inhibition that can occur between co-housed neurons (Su et
424 al., 2012; Zhang et al., 2019), the loss of these cells might not necessarily be
425 adaptive, as discussed below.
426
427 **Diverse states of neurons fated to die during antennal development**
428
429 We also discovered distinct types of undead neurons represented by cell branches in
430 the developmental trajectory of several sensilla that were present only in the PCD-
431 blocked dataset. For example, in ac3I/II sensilla – housing Or35a and either Ir75b
432 (ac3I) or Ir75c (ac3II) neurons (the lineages of these two subtypes could not be fully
433 distinguished and were considered together) – we observed two extra branches that
434 were extinguished around 30-36 h APF in control antennae but maintained in late
435 pupae in PCD-blocked antennae (Figure 5A). These clusters have a high RGS score,
436 supporting their classification as undead neurons (Figure 5B). One cluster displays a
437 signature of Naa precursor type and the other tentatively Nbb, complementing the
438 assigned Nab and Nba identities of Ir75b/Ir75c and Or35a neurons, respectively
439 (Figure 5C). We surveyed chemosensory receptors in these clusters, finding that the
440 undead Naa neuron expresses *Ir75d* (Figure 5D) – as well as *Ir* co-receptors (Figure
441 S13A) – similar to the expression of *Ir75d* in Naa neurons in ac1, ac2 and ac4
442 sensilla in wild-type antennae (Benton et al., 2025; Endo et al., 2011). We validated
443 these transcriptomic data *in situ* by demonstrating the pairing of an *Ir75d*-expressing

bioRxiv preprint doi: https://doi.org/10.1101/2025.01.16.632932; this version posted January 16, 2025. The copyright holder for this preprint (which was not certified by peer review) is the author/funder, who has granted bioRxiv a license to display the preprint in perpetuity. It is made available under aCC-BY-ND 4.0 International license.

444 neuron with Ir75b/Ir75c neurons when PCD was blocked but not in control antennae
445 (Figure 5E-G). By contrast, the undead, putative Nbb neuron did not detectably
446 express any tuning receptor, although we did observe the expression of multiple *Ir*
447 co-receptors in these cells (Figure S13A).
448 Another case of undead neuron clusters was found in sacIII sensilla, which
449 normally house Ir64a and Amt neurons. We again observed two additional cell
450 clusters in the PCD-blocked dataset with elevated RGS scores (Figure 5H-I). Here,
451 one Naa cluster expressed *Ir75d*, while in the other (of unclear precursor type) we
452 detected *Ir41a* (Figure 5J-K). In both cases, we also detected the corresponding *Ir*
453 co-receptors (Figure S13B). We confirmed *in situ* the presence of Ir75d and Ir41a
454 neurons neighboring Ir64a neurons in sacIII in PCD-blocked antennae, but not in
455 wild-type antennae (Figure 5L-N). The transcriptomic data suggested that a subset of
456 the undead Ir75d neurons might also express *Ir64a* (Figure 5K), but we did not
457 observe clear co-expression *in situ* (Figure 5L).
458 In several additional sensilla classes, we observed undead neuron populations
459 that did not detectably express any receptors (at least up to 80 h APF). In at1, in
460 addition to the *Or67d*-expressing neuron, we detected a second, Nba-derived neuron
461 in the PCD-blocked dataset (Figure 5O-R) consistent with the previous
462 electrophysiological detection of a second neuron (Prieto-Godino et al., 2020). In
463 ab10 in PCD-blocked antennae – beyond the increase in Or85f neuron numbers
464 described above – we detected an extra neuron of unclear precursor type (Figure
465 S14A-D). Finally, in ab5 and sacI, we detected very small populations of likely Naa
466 and Nbb undead neurons, respectively (Figure S14E-L).
467 Beyond these cases, for the majority of sensillar classes, we did not detect
468 clear evidence for undead neurons (e.g., ai3 and ab4) (Figure S14M-N). This was
469 surprising because, under the canonical model of the SOP lineage (Chai et al., 2019;
470 Endo et al., 2007; Endo et al., 2011), we expected all sensilla to have the potential to
471 produce four terminal cells. This might reflect a technical artefact, for example, a
472 failure to efficiently block PCD in all lineages. It is also possible that such undead
473 cells were simply not recognized as belonging to specific sensilla. This is the case for
474 any Nbb-derived glia (Endo et al., 2007; Rodrigues and Hummel, 2008; Sen et al.,
475 2005), which were not considered in our analyses. However, with two exceptions
476 (asterisk in Figure 1E, a second Ir75d neuron in ac4 (described below)), we did not
477 identify additional populations of more mature undead neurons that are not
478 associated with a particular sensillum) or with robust ectopic receptor expression. It is
479 conceivable that the canonical OSN lineage is not universal and that some sensilla
480 housing two neurons result from lack of a final cell division in the lineage, rather than
481 PCD of two of the daughters of such a division.
482
483 **Mamo is required to promote programmed cell death of Ir75d neurons**
484
485 Although PCD is the most common fate of sensory neuron precursors – if we
486 consider death as a single fate across all sensillum classes – we know essentially
487 nothing about how it is stereotypically specified. Our data indicate that transcriptional
488 activation of *rpr*, *grim* and/or *sickle* is likely to be the key inductive step, similar to
489 other tissues (Sen et al., 2004). However, very little is known about the gene
490 regulatory network upstream of these pro-apoptotic genes in any lineage, and
491 whether these are common to, or distinct between, sensilla. As a first step, we sought
492 TFs required to promote PCD in neurons in specific sensillar types, focusing first on
493 the dying lineages in ac3I/II and sacIII that both express *Ir75d*.

bioRxiv preprint doi: https://doi.org/10.1101/2025.01.16.632932; this version posted January 16, 2025. The copyright holder for this preprint (which was not certified by peer review) is the author/funder, who has granted bioRxiv a license to display the preprint in perpetuity. It is made available under aCC-BY-ND 4.0 International license.

494 Comparison of the transcriptomes of undead Ir75d neurons in the PCD-
495 blocked dataset with the normal Ir75d neurons housed in ac1, ac2 and ac4 revealed,
496 as expected, *rpr*, *grim* and *skl* to be more highly expressed in the former (Figure 6A
497 and Data S2). The gene displaying the greatest enrichment in the undead Ir75d
498 neurons was *mamo* (*maternal gene required for meiosis*) (Figure 6A). *Mamo* encodes
499 a zinc finger C2H2 protein, which we hypothesized was a PCD-promoting TF.
500 Consistently, in *mamo*^{RNAi} antennae we observed an increase in the number of *Ir75d*-
501 expressing neurons (Figure 6B). These were located both in ac3I/II (paired with
502 *Ir75b/Ir75c* expressing neurons), as well as in sacIII (paired with Ir64a neurons)
503 (Figure 6C-F). These phenotypes were not seen upon RNAi of several other TF
504 genes that have enriched expression in undead Ir75d neurons (Figure 6A and Data
505 S3).
506 The *mamo*^{RNAi} phenotype is similar to that of PCD-blocked antennae (Figure
507 5A-N) but, in principle, loss of this TF could simply lead to ectopic *Ir75d* expression in
508 another neuron type within ac3 and sacIII sensilla. Indeed, Mamo was previously
509 characterized for its role in defining cell fate in the neuroblasts (neural stem cells) of
510 the mushroom body (Liu et al., 2019). However, several observations argue against
511 this possibility in OSNs. First, in *mamo*^{RNAi} antennae the Ir75d neuron in ac3 is also
512 paired with the Or35a neuron (Figure 6G), verifying that ac3 sensilla contains distinct
513 neurons expressing Ir75b (or Ir75c), Or35a and Ir75d. Second, loss of Mamo does
514 not appear to affect fate specification of several living OSN populations in which it is
515 expressed (Figure S8), including Or35a, Ir75b, Ir75c and Ir64a neurons, although we
516 noticed modest changes in Ir75b/Ir75c and Ir64a neuron numbers upon *mamo*^{RNAi}
517 (Figure 6B). Third, we traced the projections of *Ir75d*-expressing neurons to the
518 antennal lobe using an *Ir75d promoter*-CD4:GFP reporter. In control animals, these
519 neurons converge on the VL1 glomerulus (Figure S15). A similar convergence was
520 observed in both PCD-blocked and *mamo*^{RNAi} genotypes (Figure S15), consistent
521 with both types of genetic manipulations producing equivalent undead Ir75d neurons
522 with the same projection properties as normal Ir75d neurons.
523 Together, these data implicate Mamo as part of the gene-regulatory network
524 inducing cell death of Ir75d neurons in both ac3I/II and sacIII lineages, revealing a
525 novel function of this TF. We note, however, that Mamo is expressed across a large
526 number of OSN populations (including normal Ir75d neurons in ac2) (Figure S8),
527 indicating that this TF is unlikely to be instructive alone for PCD fate but rather
528 functions in a context-dependent manner to promote death. Moreover, there also
529 appear to be Ir75d neurons that die in a *mamo*-independent manner, as inhibition of
530 PCD with P35 led to more Ir75d neurons than in *mamo*^{RNAi} antennae (Figure 6H).
531 Reviewing *Ir75d* expression patterns in PCD-blocked antennae (Figure 5E and 5L),
532 we noticed pairs of Ir75d neurons in the ac4 region. Visualizing markers for ac4
533 (Ir84a and Ir76a), we confirmed the existence of two Ir75d neurons in these sensilla
534 when PCD is blocked but not in *mamo*^{RNAi} antennae (Figure 6I-J). Thus, the ac4
535 lineage has the potential to form a second Ir75d neuron, which is normally fated to
536 die through other, unknown, TFs.
537
538 **Slp2 is required to promote programmed cell death of at1 neurons**
539
540 We next investigated the undead neuron population in at1. As we did not identify a
541 sensory receptor in this neuron to permit comparison with an endogenous cell
542 population, we sought TFs enriched in the undead cell cluster compared with the co-
543 housed Or67d neuron (Figure 7A). The at1 undead neuron exhibited higher

bioRxiv preprint doi: https://doi.org/10.1101/2025.01.16.632932; this version posted January 16, 2025. The copyright holder for this preprint (which was not certified by peer review) is the author/funder, who has granted bioRxiv a license to display the preprint in perpetuity. It is made available under aCC-BY-ND 4.0 International license.

544 expression of the forkhead TF gene *sloppy paired 2* (*slp2*) (Figure 7A-B). To examine
545 the requirement for *slp2* we performed electrophysiological recordings in at1 sensilla
546 in control and $slp2^{RNAi}$ animals, as we could not visualize the undead neuron through
547 RNA FISH for a receptor transcript. Control at1 sensilla house a single neuron,
548 detected as spikes of a uniform amplitude, corresponding to the cVA-responsive
549 Or67d neuron (Figure 7C-E). By contrast, in a large fraction of $slp2^{RNAi}$ at1 sensilla,
550 we detected an additional, smaller spike amplitude, indicative of a second, undead
551 neuron, phenocopying the consequences of blocking PCD with P35 (Figure 7C-E).
552 To further test if *slp2* activity was sufficient to promote PCD, we misexpressed
553 *slp2* in developing Or67d neurons. We used the *at1-Gal4* driver, which is selectively
554 expressed in the at1 lineage from the SOP stage until around 30 h APF, although it
555 only covers about half of the at1 SOPs (Chai et al., 2019). Strikingly, this
556 manipulation led to reduction in Or67d neuron number by around 50% (Figure 7F-G).
557 Together, these data demonstrate that Slp2 activity is necessary and sufficient to
558 promote PCD within the at1 lineage. Similar to Mamo, Slp2 was previously
559 characterized for its role in cell fate diversification within neuroblast divisions, notably
560 as part of the temporal series of TFs controlling optic lobe neuron generation
561 (Konstantinides et al., 2022; Zhu et al., 2022). It thus appears that the antennal SOP
562 lineages co-opt pleiotropic neuronal TFs as part of the gene regulatory networks that
563 promote PCD.
564
565 **Context-dependent requirement for Slp2 in promoting programmed cell death**
566
567 Beyond the undead at1 OSNs, we noticed that *slp2* is expressed in several other
568 populations of OSNs. These include those fated to die (in ab10 and ab5 sensilla),
569 lineages partially eliminated by PCD during antennal development (Or65a/b/c
570 neurons in at4 and Or85f neurons in ab10) as well as in several classes of normal
571 surviving neurons (Or19a/b, Or43a, Or69a, Or88a, Or10a/Gr10a) (Figure 8A). The
572 expression pattern of *slp2* therefore suggested a broader role for this TF in fate
573 specification in the antenna. To test this hypothesis, we surveyed the consequences
574 of $slp2^{RNAi}$ on other populations of OSNs. Loss of *slp2* had minimal or no effect on
575 Or19a, Or43a and Or69a expression (Figure 8B-C). $slp2^{RNAi}$ did however lead to
576 increases in ab10 Or85f neurons (Figure 8D-F) and at4 Or65a/b/c (Figure 8G-I)
577 neurons, restoring the 1:1 relationship with other neurons in their respective sensilla;
578 this manipulation phenocopies the effect of PCD inhibition (Figure 4F and 4I). In at4,
579 we note that Or88a neurons express appreciable levels of *slp2* (Figure 8A), but this
580 TF did not appear to have a major role in their fate specification (Figure 8H).
581 These observations argue that the contribution of Slp2 to PCD (or other
582 developmental processes) is context-specific: in some cells (e.g., the dying Nba
583 precursor in at1) it has an essential function, while in others (e.g., Or88a neurons), it
584 has little or no role. at4 Or65a/b/c neurons and ab10 Or85f neurons represent
585 intriguing intermediate cases, as they appear to undergo PCD heterogeneously in a
586 *slp2*-dependent manner. We suggest that such cases of PCD represent “collateral
587 damage” resulting from the expression of Slp2 in these cells that, perhaps due to
588 developmental noise, reaches a minimal threshold of expression to promote PCD in
589 some but not all neurons. In line with this notion, we noticed that different wild-type
590 strains exhibited varying degrees of Or65a/b/c neuron loss: w^{1118} have (like our *peb-*
591 *Gal4* strain) low numbers of Or65a/b/c neurons compared to Or47b neurons, Canton-
592 S has an equal number of these two populations, while Oregon R flies have an
593 intermediate number of Or65a/b/c neurons (Figure 8J-L). These observations are

bioRxiv preprint doi: https://doi.org/10.1101/2025.01.16.632932; this version posted January 16, 2025. The copyright holder for this preprint (which was not certified by peer review) is the author/funder, who has granted bioRxiv a license to display the preprint in perpetuity. It is made available under aCC-BY-ND 4.0 International license.

594 consistent with the possibility that this trait is not a fixed, adaptive phenotype of *D.*
595 *melanogaster*.
596
597 **Discussion**
598
599 The structural and functional properties of neural circuits are often considered as
600 optimized to fulfil their role in controlling animal behavior. In reality, however, these
601 properties represent just a snapshot in evolutionary time, neither precisely the same
602 as in the past, nor necessarily maintained in the future. Understanding the nature of
603 this snapshot in the context of a continuous process of change can offer insights into
604 how nervous systems evolve. The insect olfactory system is a particularly attractive
605 model for studying this phenomenon: this sensory system can be subject to strong
606 environmental selection pressure as the bouquet of external volatile cues changes,
607 and the typically large, rapidly reproducing populations of insect species provide the
608 necessary genetic substrate for evolutionary modifications. Using *D. melanogaster* as
609 a model, we have characterized developmental properties of OSN lineages to reveal
610 features of this species' olfactory system underlying its functional stereotypy, but also
611 how these offer the potential for evolution.
612 Through high resolution spatio-temporal transcriptomic profiling of developing
613 neurons, we first confirmed the expected global precision of receptor transcription in
614 the olfactory system, typically a single tuning receptor per neuron type. However, we
615 also reveal that this control is imperfect. We describe several examples of co-
616 expression of tuning receptors of the same or different families. Such co-expression –
617 sometimes transient – presumably reflects similarities in the gene regulatory
618 networks controlling receptor expression in distinct neuronal classes, as suggested
619 by the high degree of overlap in the set of TFs we found in different cell types. The
620 promiscuity in receptor expression is constrained, nevertheless, by the necessity to
621 have the correct complement of tuning receptor and co-receptor subunits to form a
622 functional complex. This seemingly-ectopic expression of receptor genes does permit
623 a degree of evolvability as it is possible that only transcriptional activation of a
624 complementary (co)-receptor subunit is necessary to reconstitute a functional
625 sensory receptor. However, as we have shown in two cases that artificial co-receptor
626 expression is insufficient to reconstitute function of "ectopic" tuning receptor activity,
627 we suspect that levels of ectopic tuning receptor might also need to be enhanced,
628 and there are possibly other requirements for functionality, such as perireceptor
629 proteins or morphological specializations of the neuron/sensillum.
630 Our atlas of PCD-blocked antennae allowed us to characterize the
631 development of many lineages fated to die. These lineages exhibit diverse properties:
632 the undead neurons we identified were of different precursor types within diverse
633 sensillar classes. Some of these robustly express a tuning receptor gene; here PCD
634 can counteract promiscuous receptor expression, serving as a further regulatory
635 layer to ensure precision in receptor patterning in the mature sensory system. Other
636 undead neurons lack a detectable tuning receptor; however, our detection of co-
637 receptor transcripts even in these "empty" neurons supports the idea that broad co-
638 receptor expression extends to cells destined to die, thereby reflecting a more
639 amenable evolutionary substrate for subsequent re-emergence of new neuron types
640 from such dying lineages. Why some neurons express a receptor gene and other do
641 not is an interesting open question. One possibility is that this property reflects their
642 evolutionary age: lineages that more recently evolved a PCD fate might retain the
643 gene regulatory network to permit receptor expression, while evolutionarily older

bioRxiv preprint doi: https://doi.org/10.1101/2025.01.16.632932; this version posted January 16, 2025. The copyright holder for this preprint (which was not certified by peer review) is the author/funder, who has granted bioRxiv a license to display the preprint in perpetuity. It is made available under aCC-BY-ND 4.0 International license.

644 dying lineages might have drifted in fate thus losing the capacity to express specific
645 tuning receptors. Whatever the reason, the absence of "empty" neurons in the extant
646 olfactory system implies that during emergence of a new sensory pathway from a
647 dying lineage, changes in the gene regulatory network to turn off PCD and turn on a
648 tuning receptor must be closely coordinated.
649 In this context, our identification of the first TFs (Mamo and Slp2) required for
650 specification of PCD in OSN lineages provides an important entry-point into
651 understanding how life/death fate decisions occur and evolve. The broader
652 expression of both of these TFs beyond lineages fated to die emphasizes their
653 context-dependent function, presumably because they are embedded within gene
654 regulatory networks that influence survival, death and/or differentiation of sensory
655 lineages. Further characterization of these, and other, TFs in dying lineages will help
656 reveal whether and how they directly control pro-apoptotic genes expression, and
657 why they promote PCD in some lineages but not others. Such knowledge will be key
658 to understand how patterning of PCD can change during evolution to generate or
659 remove individual sensory neuronal populations, and how this is coordinated with the
660 selective expression of receptors.
661 While several lineages are entirely condemned to death (e.g., ac3 Ir75d-
662 expressed neurons), we found, unexpectedly, that some dying neurons represent
663 subsets of normal surviving lineages (e.g., Or65a/b/c neurons in at4). Such
664 heterogeneity can be interpreted in different ways. The phenomenon might be an
665 adaptive trait, for example, to limit the numbers of just one class of neurons within a
666 specific sensillum type. However, the variation in Or65a/b/c population size across
667 different *D. melanogaster* genotypes argues against this possibility, although we
668 cannot exclude that such intraspecific phenotypic diversity arises from local
669 adaptation of specific strains. Alternatively, heterogeneous PCD might reflect
670 promiscuity in transcriptional specification of PCD resulting from overlap in gene
671 regulatory networks of surviving and dying lineages, akin to the promiscuity observed
672 in receptor expression. In this context, the observed heterogeneity in PCD
673 specification might reflect a transitory evolutionary state of these pathways, such as
674 the initial stages of loss of a sensory population. In extreme cases, promiscuous PCD
675 might result in sensilla devoid of OSNs, as observed in rare instances (Nava
676 Gonzales et al., 2021).
677 Taken together, our work both provides new understanding of the multilevel
678 mechanisms that define the functional precision of the *Drosophila* olfactory system
679 and highlights previously-overlooked variability at each of these levels that might
680 provide a substrate for the molecular and cellular changes in these sensory pathways
681 over evolutionary timescales. This study sets the stage for comparison of the
682 antennal neuronal populations of phylogenetically diverse drosophilids and other
683 insects to trace and understand the evolutionary changes in the olfactory system.
684
685

bioRxiv preprint doi: https://doi.org/10.1101/2025.01.16.632932; this version posted January 16, 2025. The copyright holder for this preprint (which was not certified by peer review) is the author/funder, who has granted bioRxiv a license to display the preprint in perpetuity. It is made available under aCC-BY-ND 4.0 International license.

Acknowledgements

We are very grateful for the invaluable assistance of the UNIL Flow Cytometry Facility and Lausanne Genomic Technologies Facility, and thank Gwénaëlle Bontonou and Roman Arguello for advice on HCR FISH. We acknowledge the Vienna *Drosophila* Resource Center, the Bloomington *Drosophila* Stock Centre (NIH P40OD018537) and the Developmental Studies Hybridoma Bank (NICHD of the NIH, University of Iowa) for reagents. We thank Nikos Konstantinides and members of the Benton laboratory for discussions and comments on the manuscript. Research in K.M.'s laboratory was supported by a National Institutes of Health award (R35GM133209). Research in R.B.'s laboratory is supported by the University of Lausanne, an ERC Advanced Grant (833548) and the Swiss National Science Foundation (310030_219185).

Author contributions

J.M. conceived the project and performed most experiments and analyses, and supervised S.C., who performed histological experiments. A.S.B. performed electrophysiological experiments in at1. D.L. contributed to initial snRNA-seq sample preparation and analyses. P.C.C. generated the *Ir75d promoter-CD4:tdGFP* transgenic line. A.J. performed electrophysiological experiments in ac4, with input from and supervision by K.M. R.B. conceived and supervised the project. J.M. and R.B. wrote the paper with input from all co-authors.

Declaration interests

The authors declare no competing interests.

Methods

Drosophila culture and transgenic line generation

Flies were reared in vials containing standard wheat flour/yeast/fruit juice medium and in incubators with 12 h light:12 h dark cycles at 25°C. Published strains are listed in Table S1.

The *Ir75d* promoter-CD4:tdGFP construct was generated by amplifying a 1994 bp DNA fragment from genomic DNA of the reference *D. melanogaster* strain (RRID:BDSC_2057) using the following forward and reverse PCR-primers GGGGACAAGTTTGTACAAAAAAGCAGGCTTCAgcaatggtaatattaaacta and GGGGACCACTTTGTACAAGAAAGCTGGGTCatccggcaactgattgcccca; this region encompasses 1850 bp 5' regulatory sequence and 144 bp of exon 1, as in a previous promoter construct (Silbering et al., 2011). The amplified sequence was inserted into pDESTHemmarG (Addgene #31221) via Gateway recombination and confirmed by sequencing. The construct was integrated into attP40 (chromosome II) using phiC31-mediated transgenesis by BestGene Inc.

Antennal dissection and nuclear isolation

10-15 virgin *peb-Gal4* females were placed in vials with 5-10 *UAS-unc84:GFP* or *UAS-p35,UAS-un84:GFP* males for 5 days, after which adults were removed. White

bioRxiv preprint doi: https://doi.org/10.1101/2025.01.16.632932; this version posted January 16, 2025. The copyright holder for this preprint (which was not certified by peer review) is the author/funder, who has granted bioRxiv a license to display the preprint in perpetuity. It is made available under aCC-BY-ND 4.0 International license.

736 pupae (corresponding to 0 h after puparium formation (APF)) were carefully
737 transferred to fresh vials and aged for 18, 24, 30, 36, 42, 48, 56, 64, 72 or 80
738 additional hours. Developing antennae from aged pupae were dissected in ice cold
739 Schneider's medium (Gibco, 21720024) and immediately transferred to 1.8 ml
740 Eppendorf tubes containing 100 µl Schneider's medium, flash-frozen in liquid
741 nitrogen and stored at -80°C. The numbers of antennae dissected in control (*peb-*
742 *Gal4/+,UAS-unc84:GFP/+*) and PCD-blocked (*peb-Gal4/+,UAS-p35/+,UAS-*
743 *unc84:GFP/+*) genotypes are as follows (time-point in h APF (n antennae control / n
744 antennae PCD-blocked): 18 (49 / 57), 24 (72 / 52), 30 (67 / 56), 36 (52 / 51), 42 (45 /
745 48), 48 (45 / 55), 56 (59 / 49), 64 (48 / 60), 72 (54 / 62) and 80 (47 / 53).
746 Samples were thawed on dry ice and nuclear suspensions prepared as
747 described (Li et al., 2022; McLaughlin et al., 2021). Suspensions from "early"
748 (18/24/30 h APF), "mid" (36/42/48 h APF) and "late" (56/64/72/80 h APF)
749 developmental time points were pooled together, with the exception of time point 80
750 h APF in the control genotype, which was pooled with mid time points. This latter
751 pooling reflected the initial experimental design, but 80 h APF control cells could be
752 effectively re-classified in the late time point for all subsequent analyses. After
753 addition of Hoechst 33342 (Thermo Fisher Scientific, 62249), samples were loaded
754 into a FACSAria flow cytometer.
755
756 **Single-nuclear RNA-sequencing**
757
758 For each pooled sample, 2 × 20,000 GFP-positive nuclei were sorted (20,000 for
759 early nuclei in PCD-blocked condition), which were immediately loaded onto the
760 Chromium Next GEM Chip (10x Genomics). Sequencing libraries were prepared with
761 the Chromium Single Cell 3□ reagent kit v3.1 dual index, following the
762 manufacturer's recommendations. Libraries were quantified by a fluorometric method
763 and quality was assessed on a Fragment Analyzer (Agilent Technologies).
764 Sequencing was performed on an Illumina NovaSeq 6000 v1.5 flow cell for 100
765 cycles according to 10x Genomics□ recommendations (28 cycles read1, 10 cycles i7
766 index read, 10 cycles i5 index, and 91 cycles read2). Demultiplexing was performed
767 with bcl2fastq2 Conversion Software (v2.20, Illumina). Raw snRNA-seq data was
768 first processed through Cell Ranger (v6.1.2, 10x Genomics) with default parameters
769 except -include introns- that was set to TRUE. A custom *D. melanogaster* reference
770 genome and transcriptome from FlyBase (Drosophila_melanogaster.BDGP6.28.101)
771 were used for mapping. Two marker genes, *GFP* and *p35*, were added to the GTF
772 and FASTA files prior to building the custom genome reference with cellranger mkref
773 (v6.1.2) function, following the 10x Genomics protocol.
774
775 **Integration of developing antennal snRNA-seq datasets from control and PCD-**
776 **blocked genotypes**
777
778 Ambient RNA contamination removal was applied on each of the cellranger output
779 matrices from early, mid and late pools in control and PCD-blocked genotypes using
780 SoupX (Young and Behjati, 2020) (v1.6.1, default parameters) and then
781 subsequently integrated and analyzed using Seurat (v4.3.0.1) in RStudio. Matrices
782 were normalized using SCTransform normalization (Hafemeister and Satija, 2019)
783 (default parameters) and integrated using reciprocal PCA workflow
784 (SelectIntegrationFeatures (nfeatures = 3000), PrepSCTIntegration,
785 FindIntegrationAnchors (reference=control) and IntegrateData) described in

bioRxiv preprint doi: https://doi.org/10.1101/2025.01.16.632932; this version posted January 16, 2025. The copyright holder for this preprint (which was not certified by peer review) is the author/funder, who has granted bioRxiv a license to display the preprint in perpetuity. It is made available under aCC-BY-ND 4.0 International license.

(https://satijalab.org/seurat/articles/integration_rpca.html). PCA was used for clustering of the integrated datasets as follows: RunPCA (npcs=50), RunUMAP (reduction="pca", dims=1:50), FindNeighbors(reduction="pca", dims=1:50), FindClusters (resolution=0.5), resulting in 49 clusters.

Cell type annotation

Marker genes (cutoff used: $log_2FC>3$) of various cell types composing the adult antenna (sensory neurons, epithelial cells, hemocytes, muscle cells, glial cells and Johnston's organ cells) were extracted from the Fly Cell Atlas dataset (Li et al., 2022) via the SCope interface (Davie et al., 2018). For support cells, *cut* and *shaven* were used as marker genes. For each cluster, the expression level (score) of cell type marker genes was computed using the AddModuleScore function implemented in Seurat. Cells were annotated through manual inspection of cell type scores in each cluster.

Neuron class annotation

OSNs and other antennal sensory neurons from the control and PCD-blocked integrated datasets were subclustered at high resolution as follows RunPCA (npcs=45), RunUMAP (reduction="pca", dims=1:45), FindNeighbors(reduction="pca", dims=1:45, k.param=10), FindClusters (resolution=6), resulting in 162 clusters. The expression of diagnostic chemosensory receptor genes in the control dataset was used for initial cluster annotation. Clusters expressing more than one diagnostic receptor were further subclustered and annotated following the same pipeline. Because chemosensory receptor gene expression occurs relatively late during antennal development, these genes could not be used alone to discriminate neuron classes at earlier developmental stages. We therefore iteratively extracted marker genes of each neuron class as follows: FindAllMarkers (assay = "SCT", logfc.threshold = 0.25, min.pct = 0.25, only.pos = T, test.use = "wilcox", p_val_adj < 0.05) and evaluated the expression level of these markers in the unannotated clusters using the AddModuleScore function. Unannotated clusters showing the highest scores for a given lineage were assigned to that lineage, which were then incorporated into the next iteration of marker extraction and scoring. In cases of conflicting scoring of various marker lists, we manually inspected the expression of few top marker genes, and privileged shortest and continuous differentiation trajectories of lineages. After three iterations (0,1,2) of cluster annotation based on individual neuron classes, further annotation of the remaining unannotated clusters was based on sensillum type by grouping co-housed OSN lineages to extract sensillar markers as follows: FindAllMarkers (assay = "SCT", logfc.threshold = 0.25, min.pct = 0.25, only.pos = T, test.use = "wilcox", p_val_adj < 0.05) followed by AddModuleScore of the various marker genes. Overall, this iterative process allowed us to annotate 90% of the neurons; the remaining unannotated fraction mostly correspond to early phase cells. Marker genes distinguishing coeloconic and sacculus neuron populations were extracted from (Corthals et al., 2023; Mika et al., 2021). Gene expression levels shown in the dot plots and UMAPs are residuals from a regularized negative binomial regression, and have arbitrary units.

bioRxiv preprint doi: https://doi.org/10.1101/2025.01.16.632932; this version posted January 16, 2025. The copyright holder for this preprint (which was not certified by peer review) is the author/funder, who has granted bioRxiv a license to display the preprint in perpetuity. It is made available under aCC-BY-ND 4.0 International license.

836 **Lineage developmental and pseudotime reconstruction**
837
838 Individual sensillar lineages were extracted from the integrated datasets and
839 subclustered using a similar workflow as described above but with lineage-specific
840 parameters: RunPCA, RunUMAP, FindNeighbors, FindClusters. Each cluster was
841 assigned to early, mid and late developmental phases based on PCD-blocked data
842 and then extrapolated to the control data (this was necessary, due to the pooling of
843 the 80 h APF time point with the mid stages in the latter). Individual lineages were
844 imported in monocle3 (v1.2.9) (Cao et al., 2019; Levine et al., 2015; Qiu et al., 2017;
845 Trapnell et al., 2014) and pseudotime inferred as follows: cluster_cells, learn_graph
846 (use_partition = F), order_cells (start_end was chosen at the tip of "early" stage cells)
847 and gene expression dynamics plotted using plot_genes_in_pseudotime
848 (color_cells_by = "pseudotime") function.
849
850 **Identification of undead neurons**
851
852 During reconstruction of individual lineages, we systematically checked for the
853 presence of clusters that would be exclusive to the PCD-blocked dataset using
854 DimPlot (split.by = "condition") function in Seurat. We confirmed that any such PCD-
855 blocked specific clusters corresponded to undead neuron lineages by quantifying the
856 expression of the pro-apoptotic genes *rpr*, *grim* and *skl* (RGS score) using
857 AddModuleScore function. If there was no difference in clusters between control and
858 PCD-blocked animals, we quantified the number of cells (from 36 h APF) of each
859 lineage in both conditions. In a few cases (e.g., at4 Or65a/b/c neurons) there was a
860 clear increase in number in the PCD-blocked dataset. We further validated such
861 additional cells as being undead neurons, by quantifying and ranking RGS score at
862 the sensillar level using AddModuleScore, ViolinPlot (features = "RGS", sort = T)
863 function. Typically, lineages with "embedded" undead neurons had the highest RGS
864 score.
865
866 **Differential gene expression analysis**
867
868 Differentially expressed genes (DEGs) were extracted from various Seurat objects
869 using FindAllMarkers function with the following parameters applied for various
870 comparisons: for developmental time marker genes (Figure S2): (object = "All
871 OSNs", assay = "SCT", logfc.threshold = 0.25, min.pct = 0.25, only.pos = T, test.use
872 = "wilcox", p_val_adj < 0.05), for OSN marker genes (Figure S5): (object = "All
873 annotated OSNs in control condition", assay = "SCT", logfc.threshold = 0.25, min.pct
874 = 0.18, only.pos = T, test.use = "wilcox", p_val_adj < 0.05), for sensilla marker genes
875 (Figure S6): (object = "All annotated OSNs in control condition", assay = "SCT",
876 logfc.threshold = 0.25, min.pct = 0.25, only.pos = T, test.use = "wilcox", p_val_adj <
877 0.05), for OSN precursor type marker genes (Figure S7): (object = "All annotated
878 OSNs in control condition except arista", assay = "SCT", logfc.threshold = 0.25,
879 min.pct = 0.4, only.pos = T, test.use = "wilcox", p_val_adj < 0.05). For each
880 comparison, an analysis of Gene Ontology terms over-represented in marker genes
881 was performed using clusterProfiler (v4.4.4) (Wu et al., 2021).
882
883

bioRxiv preprint doi: https://doi.org/10.1101/2025.01.16.632932; this version posted January 16, 2025. The copyright holder for this preprint (which was not certified by peer review) is the author/funder, who has granted bioRxiv a license to display the preprint in perpetuity. It is made available under aCC-BY-ND 4.0 International license.

884 **Hierarchical clustering of sensory neurons based on differentially expressed**
885 **transcription factors**
886
887 A phylogenetic tree relating sensory neuron classes (Figure 3L) was built based on a
888 distance matrix constructed in the differentially expressed transcription factors
889 (DE_TFs) space (Figure S8) using the BuildClusterTree function implemented in
890 Seurat: BuildClusterTree (assay = "SCT", features = DE_TFs).
891
892 **Hybridization chain reaction RNA fluorescent *in situ***
893
894 RNA probes (Table S2) were synthesized by Molecular Instruments, and we followed
895 a published HCR RNA FISH protocol (Bontonou et al., 2024) with minor
896 modifications. Female flies (2-7 days old) of interest were flash-frozen in liquid
897 nitrogen and antennae were passed through a mini-sieve (mesh-width = 80 μm) and
898 collected in Petri dishes containing fixation solution (1×PBS, 3% Triton X-100, 4%
899 paraformaldehyde). For each staining, 30-40 antennae were immediately transferred
900 into 1.5 ml Eppendorf tubes filled with 1 ml of fixation solution and place on a
901 platform for 1 h at room temperature (RT) with gentle shaking (35 rpm). Fixative
902 solution was removed and samples washed 2× 5 min with 1 ml of PBS 1×, 3% Triton
903 X-100 at RT, followed by 3× 5 min with 1 ml of 1×PBS, 0.1% Triton X-100 at RT.
904 Wash solution was removed and samples pre-hybridized with 300 μl of probe
905 hybridization buffer (Molecular Instruments) for 30 min at 37°C. Pre-hybridization
906 buffer was removed and replaced by probe solution (5 μl of probe in hybridization
907 solution, 500 μl final volume, except for *Ir75d*, *Ir41a*, *Or85f*, *Or88a, Or67d* and *Ir76a*
908 probes for which 10 μl were used) for 16 h at 37°C. Probe solution was removed and
909 samples washed 4× 15 min with 500 μl of pre-heated (37°C) probe wash buffer
910 (Molecular Instruments) at 37°C, followed by 3× washes of 5 min at RT with 500 μl of
911 5×SSCT solution (5×SSC, 0.1% Triton X-100). Samples were pre-amplified with 300
912 μl of amplification buffer (Molecular Instruments) for 30 min at RT. During this time,
913 for each probe in a sample, 10 μl of hairpin amplifiers h1 and 10 μl of hairpin
914 amplifiers h2 (or 15 μl each when probe volume was doubled) were heated at 95°C
915 for 90 s, and snap-cooled to RT, with protection from light. Pre-amplification buffer
916 was removed from the samples and replaced by the snap-cooled amplifiers in
917 amplification buffer (Molecular Instruments), 500 μl final volume, and placed at RT
918 and protected from light for 16 h. Amplification solution was removed and samples
919 washed 5× in 500 μl of 5×SSCT at RT (2× 5 min, 2× 30 min and 1× 5 min). 5×SSCT
920 was removed and 50 μl of Vectashield mounting medium (Vector Laboratories, H-
921 1200) was added before mounting.
922
923 **Standard RNA fluorescent *in situ* hybridization and immunohistochemistry**
924
925 For the experiments in Figure 6G, we used a standard RNA FISH protocol (Saina
926 and Benton, 2013) on female flies (2-7 day old), using RNA FISH probes generated
927 using primers in Table S2. When combined with immunohistochemistry (Figure
928 S15A), we performed standard RNA FISH until TSA-Cy5 colorimetric detection,
929 when samples were washed 5× 20 min at RT with 500 μl of TNT buffer and
930 incubated for 1 h in 300 μl of blocking solution (1×PBS, 0.2% Triton X-100, 5% heat
931 inactivated goat serum). Supernatant was replaced by 500 μl of anti-GFP-chicken
932 antibody containing blocking solution and samples placed at 4°C on a rotating wheel

bioRxiv preprint doi: https://doi.org/10.1101/2025.01.16.632932; this version posted January 16, 2025. The copyright holder for this preprint (which was not certified by peer review) is the author/funder, who has granted bioRxiv a license to display the preprint in perpetuity. It is made available under aCC-BY-ND 4.0 International license.

933 for 40 h. Samples were then washed 5× 20 min at RT with 500 µl of 1×PBS, 0.2%
934 Triton X-100, and incubated for 1 h in 300 µl of blocking solution. Supernatant was
935 replaced by 500 µl of secondary antibodies in blocking solution and samples placed
936 at 4°C on a rotating wheel for 40 h. Samples were washed 5× 20 min at RT with 500
937 µl of 1×PBS, 0.2% Triton X-100 and 50 µl of Vectashield mounting medium (Vector
938 Laboratories, H-1200) was added to each sample prior to mounting. Primary and
939 secondary antibodies are listed in Table S3.
940
941 **Immunohistochemistry in central brain**
942
943 Female flies (2-7 day old) were fixed in 2 ml of PB 1×, 3% Triton X-100, 4%
944 paraformaldehyde for 2 h at RT. Brains were dissected into ice-cold 1×PB (under a
945 binocular microscope and immediately transferred into 1.5 ml Eppendorf tubes
946 containing 1 ml of 1×PB, 0.3% Triton X-100. Brains were washed 5× 15 min in 1 ml
947 of 1×PB, 0.3% Triton X-100 at RT, and then incubated in 1 ml of blocking solution
948 (PB 1×, 0.3% Triton X-100, 5% heat-inactivated goat serum) for 1 hat RT.
949 Supernatant was replaced by 500 µl of primary antibodies in blocking solution and
950 the samples placed on a rotating wheel for 40 h at 4°C. Brains were washed 5× 15
951 min in 1 ml of 1×PB, 0.3% Triton X-100 at RT, and then incubated in 1 ml of blocking
952 solution for 1 h at RT. The supernatant was replaced by 500 µl of secondary
953 antibodies containing blocking solution and the samples placed on a rotating wheel
954 for 40 h at 4°C. Brains were washed 5× 15 min in 1 ml of 1×PB, 0.3% Triton X-100 at
955 RT, and 50 µl of Vectashield mounting medium (Vector Laboratories, H-1200) was
956 added prior to mounting.
957
958 **Image acquisition and processing**
959
960 Images from antennae and antennal lobes were acquired with confocal microscopes
961 (Zeiss LSM710 or Zeiss LSM880 systems) using a 40× (antennae) or a 63×
962 (antennal lobe) oil immersion objective. Images were processed using Fiji software
963 (Schindelin et al., 2012).
964
965 **Electrophysiology**
966
967 Single-sensillum recordings on ac4 coeloconic sensilla were performed on 2-4 day
968 old female flies using glass electrodes filled with sensillum recording solution,
969 essentially as described (Vulpe et al., 2021). Coeloconic sensilla were identified
970 based on their stereotyped locations on the antenna and responses to diagnostic
971 odorants. The odor response was calculated from the difference in summed spike
972 frequencies of all OSNs in response to a 0.5 s odor puff compared to a 0.5 s solvent
973 puff, as described (Vulpe et al., 2021).
974 Single sensillum recordings from at1 were performed on 5-10-day old female
975 flies using tungsten electrodes, essentially as described (Benton and Dahanukar,
976 2023); sensilla were identified by their morphology, characteristic location and
977 responses of Or67d neuron to cVA. Odor responses were calculated from the
978 difference between the OSN spike frequency during and before odor stimulation, as
979 described (Benton et al., 2007), from which the solvent response was subtracted.
980 Spike amplitudes numbers in at1 (Figure 7D) were scored independently by two

bioRxiv preprint doi: https://doi.org/10.1101/2025.01.16.632932; this version posted January 16, 2025. The copyright holder for this preprint (which was not certified by peer review) is the author/funder, who has granted bioRxiv a license to display the preprint in perpetuity. It is made available under aCC-BY-ND 4.0 International license.

981 experimenters blind to the genotype. Information on odor stimuli and the paraffin oil
982 solvent is provided in Table S4.
983

bioRxiv preprint doi: https://doi.org/10.1101/2025.01.16.632932; this version posted January 16, 2025. The copyright holder for this preprint (which was not certified by peer review) is the author/funder, who has granted bioRxiv a license to display the preprint in perpetuity. It is made available under aCC-BY-ND 4.0 International license.

984 **Supplementary Information**
985
986 **Data S1. Odor-evoked neuronal responses.**
987 *- see separate Excel file*
988
989 **Data S2. Top marker genes in undead and normal Ir75d neurons.**
990 *- see separate Excel file*
991
992 **Data S3. RNAi screen data.**
993 *- see separate Excel file*
994
995 **Table S1. *Drosophila* strains.**
996

Genotype	Source/reference
w^{1118}	
Canton S	
Oregon R	
peb-Gal4	RRID:BDSC_80570
UAS-unc84:GFP	RRID:BDSC_602372
UAS-p35	RRID:BDSC_5072
UAS-Dcr-2	VDRC_60010
UAS-$mamo^{RNAi}$	VDRC_110310
UAS-lz^{RNAi}	VDRC_330539
UAS-lbe^{RNAi}	VDRC_102377
UAS-lbl^{RNAi}	VDRC_52323
UAS-Orco	(Benton et al., 2006)
UAS-Ir8a	(Abuin et al., 2011)
Or67d-Gal4	(Kurtovic et al., 2007)
Ir84a-Gal4	(Grosjean et al., 2011)
at1-Gal4 (GMR82D08-Gal4)	(Chai et al., 2019)
UAS-slp2-ORF-3HA	FlyORF

997
998 **Table S2. RNA FISH probes.**
999

Gene	Reference/source	Primer sequences (5'-3' Fwd / Rev) (standard FISH) or target sequence (HCR-FISH)
Amt	Molecular Instruments	NM_001104330.3
Ir41a	Molecular Instruments	NM_206022.4
Ir64a	Molecular Instruments	NM_139705.1
Ir75b	Molecular Instruments	KY205710.1
Ir75d	Molecular Instruments	NM_140817.3
Ir76a	Molecular Instruments	NM_001104177.3
Ir84a	Molecular Instruments	NM_141463.2
Ir92a	Molecular Instruments	NM_001104375.2
lbe	Molecular Instruments	NM_079711.3
lbl	Molecular Instruments	NM_079710.4
lz	Molecular Instruments	NM_078544.3
Or19a	Molecular Instruments	NM_080274.3

bioRxiv preprint doi: https://doi.org/10.1101/2025.01.16.632932; this version posted January 16, 2025. The copyright holder for this preprint (which was not certified by peer review) is the author/funder, who has granted bioRxiv a license to display the preprint in perpetuity. It is made available under aCC-BY-ND 4.0 International license.

Or23a	Molecular Instruments	NM_078734.4
Or35a	Molecular Instruments	NM_165117.2
Or43a	Molecular Instruments	NM_078923.3
Or47b	Molecular Instruments	NM_078966.3
Or65a	Molecular Instruments	NM_168163.1
Or67a	Molecular Instruments	NM_079281.4
Or67b	Molecular Instruments	NM_079283.5
Or67d	Molecular Instruments	NM_140133.2
Or69a	Molecular Instruments	NM_206348.1
Or83c	Molecular Instruments	NM_079520.3
Or85f	Molecular Instruments	NM_079565.3
Or88a	Molecular Instruments	NM_079624.3
Ir75b		CCGCATCTATGTGGAAACCT / CAATATGCCCATGCAGAGAA
Or35a		TAGCTGTGCGATGTCTTG / GTCAAAAGCAGTGGCACAAA
Ir75d		GACAGGATCTGGAGGGCATA / ACACCCACACATCGTTCTCA

1000
1001 **Table S3. Antibodies.**
1002

Antibody	Dilution	Reference/source	Identifier
Chicken anti-GFP	1:500	Abcam	ab13970
Mouse anti-Bruchpilot (nc82)	1:10	DSHB	nc82
anti-DIG-POD	1:300	Roche Diagnostics AG	11 207 733 910
anti-Fluorescein-POD	1:300	Roche Diagnostics AG	11 426 346 910
Alexa Fluor 488 Goat anti-Chicken	1:500	Abcam	ab150169
Cy5 Goat anti-Mouse	1:250	Jackson Immunoresearch	115-175-166

1003
1004 **Table S4. Odors.**
1005

Odor	CAS	Source
11-cis-vaccenyl acetate (cVA)	6186-98-7	Pherobank
E2-hexenal	6728-26-3	Sigma-Aldrich
1-hexanol	111-27-3	Acros Organics
hexyl acetate	142-92-7	Sigma-Aldrich
1-octanol	111-87-5	Acros Organics
2-oxopentanoic acid	1821-02-9	Sigma-Aldrich
paraffin oil (solvent)	8012-95-1	Acros Organics
phenethylamine	64-04-0	Acros Organics
phenylacetaldehyde	122-78-1	Alfa Aesar

1006

bioRxiv preprint doi: https://doi.org/10.1101/2025.01.16.632932; this version posted January 16, 2025. The copyright holder for this preprint (which was not certified by peer review) is the author/funder, who has granted bioRxiv a license to display the preprint in perpetuity. It is made available under aCC-BY-ND 4.0 International license.

1007 **Figure Legends**
1008
1009 **Figure 1. A developmental atlas of antennal sensory neurons.**
1010 **(A)** Schematic of the development and anatomy of the *D. melanogaster* peripheral
1011 olfactory system.
1012 **(B)** Schematic of experimental design: antennal imaginal discs/antennae were
1013 dissected at time points every 6-8 h from 18-80 h after puparium formation (APF) in
1014 control (*peb-Gal4/+;;UAS-unc84:GFP/+*) and PCD-blocked (*peb-Gal4/+;UAS-*
1015 *p35/+;UAS-unc84:GFP/+*) conditions. Samples were pooled into three temporal
1016 phases (early, mid, late) prior FACS sorting and 10x sequencing. Tapered black bars
1017 indicate the timing of the main developmental processes.
1018 **(C)** UMAP of all cell types in the developmental atlas, integrating control and PCD-
1019 blocked datasets.
1020 **(D)** UMAP of all olfactory sensory neurons in (C) in the atlas – integrating control and
1021 PCD-blocked datasets – colored by developmental phases.
1022 **(E)** UMAP of annotated neuronal lineages, integrating control and PCD-blocked
1023 datasets. Unannotated neurons could not be assigned to any lineage; almost all of
1024 these are from early developmental stages, but one cluster (specific to the PCD-
1025 blocked dataset) was detected in late developmental stages (asterisk, close to the
1026 Amt-ac1 lineage). Some *repo* expressing glial cells were also detected (see Figure
1027 S3A-B).
1028 **(F)** UMAP of the cells in (E) – masking unannotated neurons and glial cells – colored
1029 by sensillar class (ab, antennal basiconic; at, antennal trichoid; ai, antennal
1030 intermediate; ac, antennal coeloconic; sac, sacculus).
1031 **(G)** UMAP of the cells in (F) – now also masking cells from the PCD-blocked dataset
1032 and dying and aristal lineages from the control dataset – colored by neuron precursor
1033 type (aristal lineages could not be confidently assigned to any type).
1034 **(H)** Scatter plot of the relative abundance of each neuronal population in the
1035 developmental atlas (control dataset only) with their relative abundance as quantified
1036 *in situ* (Benton et al., 2025).
1037
1038 **Figure 2. Novel lineage-specific transcription factors.**
1039 **(A)** Expression of the TFs *lozenge* (*lz*), *ladybird early* (*lbe*) and *ladybird late* (*lbl*) as
1040 well as *Or85f*, *Or67a*, *Or83c* and *Or23a* across cell types (control dataset, except
1041 dying lineages, here and in other panels). Expression levels (here and elsewhere)
1042 have arbitrary units (see Methods).
1043 **(B)** UMAPs highlighting the ab10 lineages (schematized in the cartoon) (left) and the
1044 expression of the indicated genes (right).
1045 **(C)** Expression of the indicated genes in ab10 cells grouped by developmental
1046 phases.
1047 **(D)** UMAPs highlighting the ai2 lineages (schematized in the cartoon) (left) and the
1048 expression of the indicated genes (right).
1049 **(E)** Expression of the indicated genes in ai2 cells grouped by developmental phases.
1050 **(F)** RNA FISH on whole-mount antennae of control (*peb-Gal4*) animals with the
1051 indicated probes (*n* = 10-16 antennae). Scale bars, 25 µm (or 10 µm for single
1052 confocal Z-slice, high-magnification images on the right), here and in other panels.
1053 **(G)** RNA FISH on whole-mount antennae of control (*peb-Gal4,UAS-Dcr2*) and *lz*^{RNAi}
1054 (*peb-Gal4,UAS-Dcr-2/+;UAS-lz*^{RNAi}*/+;*) animals with probes targeting the indicated
1055 transcripts.

bioRxiv preprint doi: https://doi.org/10.1101/2025.01.16.632932; this version posted January 16, 2025. The copyright holder for this preprint (which was not certified by peer review) is the author/funder, who has granted bioRxiv a license to display the preprint in perpetuity. It is made available under aCC-BY-ND 4.0 International license.

1056 **(H)** Quantification of experiments in (G), together with a control *Or67b* probe (images
1057 not shown). Here and elsewhere, box plots illustrate individual data points overlaid on
1058 boxes showing the median (thick line), first and third quartiles, while whiskers indicate
1059 data distribution limits. *n* is indicated underneath. *** = P < 0.001; ns = P > 0.05,
1060 respectively, *t* test.
1061 **(I)** RNA FISH on whole-mount antennae of control (*peb-Gal4*) animals with the
1062 indicated probes (*n* = 10-16 antennae).
1063 **(J)** RNA FISH experiment on whole-mount antennae of control (*peb-Gal4,UAS-Dcr-*
1064 *2*), *lbl*^{RNAi} (*peb-Gal4,UAS-Dcr-2/+;;UAS-lbl*^{RNAi}/+), *lbe*^{RNAi} (*peb-Gal4,UAS-Dcr-*
1065 *2/+;UAS-lbe*^{RNAi}/+;), and *lbl*^{RNAi}*,lbe*^{RNAi} (*peb-Gal4,UAS-Dcr2/+;UAS-lbe*^{RNAi}/+*;UAS-*
1066 *lbl*^{RNAi}/+) animals with the indicated probes targeting the indicated transcripts.
1067 **(K)** Quantification of experiments in (J), together with a control *Or43a* probe (images
1068 not shown). *n* is indicated underneath. * = P < 0.05; ** = P < 0.01; *** = P < 0.001;
1069 Wilcoxon rank sum test followed by Bonferroni correction for multiple comparisons.
1070 ns = P > 0.05, *t* test.
1071

1072 **Figure 3. Precision and promiscuity of sensory receptor transcription.**
1073 **(A)** Dot plot illustrating the expression of tuning receptor and co-receptor subunits
1074 across sensory neuron types in the late-stage, control dataset (*peb-Gal4/+;;UAS-*
1075 *unc84:GFP/+*). Only three expected tuning receptors were not detected: (i) *Or49a*
1076 (which was, however, detectable in the expected cells – i.e., co-expressed with *Or85f*
1077 – in the non-normalized data (not shown), (ii) co-expressed *Or10a* and *Gr10a* (likely
1078 because the genes have identical annotations, resulting in reads being filtered out
1079 due to unintended mapping to two distinct genes), and (iii) Or33b, which were not
1080 detected in Or85a neurons as reported (Fishilevich and Vosshall, 2005), but instead
1081 detected in a very small fraction of Or56a/Or33a neurons, potentially reflecting strain
1082 specificity.
1083 **(B)** Top: UMAPs of the ac4A lineage illustrating the developmental stages and
1084 receptor expression patterns (control dataset). Bottom: a pseudotime UMAP and
1085 corresponding receptor expression dynamics.
1086 **(C)** RNA FISH on whole-mount antennae of control (*peb-Gal4*) animals with probes
1087 targeting the indicated transcripts (*n* = 10-12). The ac3 and ac4 sensilla zones are
1088 indicated in the top and middle rows. Bottom: ac4A neurons co-expressing *Ir84a* and
1089 *Or35a* and ac4B neurons co-expressing *Ir76a* and *Or35a* in a single confocal Z-slice.
1090 Scale bars, 25 µm (top and middle rows) or 10 µm (bottom row).
1091 **(D)** Electrophysiological responses to the indicated ligands in ac4 sensilla from
1092 antennae of control animals (*UAS-Orco*) and animals overexpressing *Orco* in ac4A
1093 neurons (*Ir84a*^{Gal4}*/UAS-Orco*). Solvent-corrected responses (mean ± SEM) are
1094 shown; see Data S1 for raw data and statistical analyses.
1095 **(E)** Schematic summarizing tuning receptor (black) and co-receptor (grey) subunits
1096 expressed in ac4 neurons.
1097 **(F)** UMAPs of the ab5B (top rows) or at1 (bottom rows) lineages illustrating the
1098 developmental stages and receptor expression patterns (control dataset),
1099 pseudotime UMAPs and corresponding receptor expression dynamics.
1100 **(G)** Electrophysiological responses to the indicated ligands in at1 sensilla from
1101 antennae of control animals (*UAS-Ir8a*) and animals overexpressing *Ir8a* in at1
1102 neurons (*Or67d-Gal4/UAS-Ir8a*). Solvent-corrected responses (mean ± SEM) are
1103 shown; see Data S1 for raw data and statistical analyses.

bioRxiv preprint doi: https://doi.org/10.1101/2025.01.16.632932; this version posted January 16, 2025. The copyright holder for this preprint (which was not certified by peer review) is the author/funder, who has granted bioRxiv a license to display the preprint in perpetuity. It is made available under aCC-BY-ND 4.0 International license.

1104 **(H)** Hierarchical clustering of antennal neuron types based upon differentially
1105 expressed TFs (from Figure S8).
1106
1107 **Figure 4. Heterogeneous life and death fates of specific OSN populations.**
1108 **(A)** Schematic of the programmed cell death cascade in *D. melanogaster*.
1109 **(B)** UMAPs illustrating the combined expression levels of the pro-apoptotic genes
1110 *reaper* (*rpr*), *grim* and *sickle* (*skl*) – quantified as a "RGS" score – in control (*peb-*
1111 *Gal4/+;;UAS-unc84:GFP/+*) and PCD-blocked (*peb-Gal4/+;UAS-p35/+;UAS-*
1112 *unc84:GFP/+*) datasets.
1113 **(C)** RGS score in control and PCD-blocked datasets. Here and elsewhere, boxes
1114 show the median (thick line), first and third quartiles, while whiskers indicate data
1115 distribution limits. **** = P < 0.0001, Wilcoxon rank sum test.
1116 **(D)** Abundance of ab4, ab7, ab10 and at4 neuronal classes in control (yellow) and
1117 PCD-blocked (blue) datasets, calculated as the percentage of nuclei for each class
1118 relative to the total number of nuclei (from 36 h APF, excluding those forming new
1119 clusters in the PCD-blocked dataset).
1120 **(E)** Reconstruction of the ab10 sensillum development in the integrated control and
1121 PCD-blocked datasets. Cells were extracted from the datasets using sensillar
1122 markers (Figure 1F and Figure S6), and reclustered (see Methods); note in these
1123 UMAPs we mask a cell cluster that is unique to the PCD-blocked dataset, which is
1124 considered further in Figure S14A-C. UMAPs indicate the identity and the
1125 developmental phases (top), the expression of olfactory receptors (middle) and RGS
1126 score within the lineage (bottom). Boxplot indicates the ranked (left > right) RGS
1127 score in ab10 neurons (**** = P < 0.0001, Wilcoxon rank sum test).
1128 **(F)** RNA FISH on whole-mount antennae of control (*peb-Gal4*) and PCD-blocked
1129 animals (*peb-Gal4/+;UAS-p35/+*) with probes targeting the indicated transcripts.
1130 Scale bars, 25 µm. Quantifications are shown on the right.
1131 **(G)** Schematic of the inferred subtypes of ab10 sensilla in control and PCD-blocked
1132 datasets.
1133 **(H)** Reconstruction of the at4 sensillum development in the integrated control and
1134 PCD-blocked datasets. UMAPs indicate the identity and the developmental phases
1135 (top), the expression of olfactory receptors (middle) and RGS score within the lineage
1136 (bottom). Boxplot indicates the ranked (left > right) RGS score in at4 neurons.
1137 **(I)** RNA FISH on whole-mount antennae of control (*peb-Gal4*) and PCD-blocked
1138 animals (*peb-Gal4/+;UAS-p35/+*) with probes targeting the indicated transcripts.
1139 Scale bars, 25 µm. Quantifications are shown on the right.
1140 **(J)** Schematic of the inferred subtypes of at4 sensilla in control and PCD-blocked
1141 datasets.
1142 **(F, H and I)** A, B and C indicate significant differences: P < 0.05 in pairwise
1143 comparisons (Wilcoxon rank sum test followed by Bonferroni correction for multiple
1144 comparisons).
1145
1146 **Figure 5. Identification of novel populations of undead neurons.**
1147 **(A)** UMAPs of the ac3I/II lineages in control and PCD-blocked datasets illustrating the
1148 developmental stages (top) and RGS expression (bottom), revealing cells with high
1149 RGS score that are present exclusively in PCD-blocked animals.
1150 **(B)** Left: lineage annotation of ac3I/II sensilla in integrated control and PCD-blocked
1151 data. Right: ranked RGS scores.
1152 **(C)** Neuron precursor type score for each OSN in the ac3I/II integrated dataset.

bioRxiv preprint doi: https://doi.org/10.1101/2025.01.16.632932; this version posted January 16, 2025. The copyright holder for this preprint (which was not certified by peer review) is the author/funder, who has granted bioRxiv a license to display the preprint in perpetuity. It is made available under aCC-BY-ND 4.0 International license.

1153 **(D)** UMAPs of the integrated ac3I/II dataset illustrating the expression of sensory
1154 receptors in endogenous and undead neurons.
1155 **(E)** RNA FISH on whole-mount antennae of control (*peb-Gal4*, top row) and PCD-
1156 blocked animals (*peb-Gal4/+;UAS-p35/+;* bottom row) with probes targeting the
1157 indicated transcripts. The ac3 zone is indicated. Right column images show a higher
1158 magnification of single confocal Z-slice in the ac3 zone. Scale bars, 25 μm (left
1159 images) or 10 μm (right images).
1160 **(F)** Quantification of OSN numbers from the experiments in (E) (*n* is indicated
1161 underneath). *** indicates P < 0.001, *t* test.
1162 **(G)** Schematic of the inferred types of ac3I/II sensilla in control and PCD-blocked
1163 antennae.
1164 **(H)** UMAPs of the sacIII-v/d lineages in control and PCD-blocked datasets illustrating
1165 the developmental stages (top) and RGS expression (bottom), revealing cells with
1166 high RGS score that are present exclusively in PCD-blocked animals.
1167 **(I)** Left: lineage annotation of sacIII-v/d sensilla in integrated control and PCD-
1168 blocked data. Right: ranked RGS scores.
1169 **(J)** Neuron precursor type score for each OSN in the sacIII-v/d integrated dataset.
1170 **(K)** UMAPs of the integrated sacIII-v/d dataset illustrating the expression of sensory
1171 receptors in endogenous and undead neurons.
1172 **(L)** RNA FISH on whole-mount antennae of control (*peb-Gal4*, top row) and PCD-
1173 blocked animals (*peb-Gal4/+;UAS-p35/+;* bottom row) with probes targeting the
1174 indicated transcripts. The sacIII zone is indicated. Right column images show a
1175 higher magnification of single confocal Z-slice in the sacIII zone. Scale bars, 25 μm
1176 (left images) or 10 μm (right images).
1177 **(M)** Quantification of OSN numbers from the experiments in (L) (*n* is indicated
1178 underneath). *** indicates P < 0.001, *t* test.
1179 **(N)** Schematic of the inferred states of sacIII-v/d sensilla in control and PCD-blocked
1180 antennae.
1181 **(O)** UMAPs of the at1 lineages in control and PCD-blocked datasets illustrating the
1182 developmental stages (top) and RGS expression (bottom), revealing cells with high
1183 RGS score that are present exclusively in PCD-blocked animals.
1184 **(P)** Top: lineage annotation of the at1 sensillum in control and PCD-blocked
1185 integrated data. Bottom: ranked RGS scores (left) and precursor type scores (right).
1186 **** indicates P < 0.0001, Wilcoxon rank sum test.
1187 **(Q)** Endogenous expression of *Or67d* in the control and PCD-blocked integrated
1188 data. No receptor was robustly detected in the undead neuron population.
1189 **(R)** Schematic of the inferred states of the at1 sensillum in control and PCD-blocked
1190 antennae.
1191 **(B,C,I,J)** A-D letters indicate significant differences: P < 0.05 in pairwise comparisons
1192 (Wilcoxon rank sum test followed by Bonferroni correction for multiple comparisons).
1193

1194 **Figure 6. *Mamo* specifies PCD in Ir75d neuron lineages.**
1195 **(A)** Volcano plot illustrating differentially-expressed genes between undead Ir75d
1196 OSNs (in ac3 and sacIII) and normal Ir75d OSNs (in ac1, ac2 and ac4) (pseudobulk
1197 analysis, *x* axis = $\log_2$FC("undead"/control), *y* axis = -$\log_{10}$(adjusted P), $\log_2$FC >
1198 0.25, % of positive nuclei > 0.25). Pro-apoptotic genes are highlighted in blue, and
1199 TFs whose expression is enriched in the undead Ir75d neurons are highlighted in red.
1200 See Data S2 for the top 20 genes enriched in undead and living Ir75d neuron
1201 counterparts.

bioRxiv preprint doi: https://doi.org/10.1101/2025.01.16.632932; this version posted January 16, 2025. The copyright holder for this preprint (which was not certified by peer review) is the author/funder, who has granted bioRxiv a license to display the preprint in perpetuity. It is made available under aCC-BY-ND 4.0 International license.

1202 **(B)** Quantification of OSN numbers in the indicated genotypes (*n* is indicated
1203 underneath). *** indicates P < 0.001, *t* test.
1204 **(C,D)** RNA FISH on whole-mount antennae of control (*peb-Gal4,UAS-Dcr-2*, top row)
1205 and *mamo*^{RNAi} animals (*peb-Gal4,UAS-Dcr-2/+;UAS-mamo*^{RNAi}*/+*, bottom row) with
1206 probes targeting the indicated transcripts. ac3 (C) and sacIII (D) zones are shown.
1207 Right column images show a higher magnification within the ac3 and sacIII zones of
1208 a single confocal Z-slice, showing "undead" Ir75d neurons upon *mamo*^{RNAi} in both
1209 ac3 and sacIII sensilla. Scale bars, 25 µm (left images) or 10 µm (right images).
1210 **(E,F)** Schematic of the inferred states of ac3I/II (E) and sacIII-v/d (F) sensilla in
1211 control and *mamo*^{RNAi} conditions.
1212 **(G)** RNA FISH on whole-mount antennae of control (*peb-Gal4,UAS-Dcr-2;* top) and
1213 *mamo*^{RNAi} animals (*peb-Gal4,UAS-Dcr-2/+;UAS-mamo*^{RNAi}*/+;* bottom) with probes
1214 targeting the indicated transcripts. The ac3 zone is indicated. Right column images
1215 show a higher magnification in the ac3 zone in a single confocal Z-slice. Scale bars,
1216 25 µm, or 10 µm for high-magnification images.
1217 **(H)** Quantification of Ir75d neurons in the indicated genotypes (*n* is indicated
1218 underneath); data is replotted from Figures 5K and 6B, to highlight the mismatch of
1219 Ir75d neuron numbers in *mamo*^{RNAi} and PCD-blocked animals. A-C letters indicate
1220 significant differences: P < 0.05 in pairwise comparisons (Wilcoxon rank sum test
1221 followed by Bonferroni correction for multiple comparisons).
1222 **(I)** RNA FISH on whole-mount antennae of PCD-blocked (*peb-Gal4/+;UAS-p35/+;*
1223 *left*) and *mamo*^{RNAi} animals (*peb-Gal4,UAS-Dcr-2/+;UAS-mamo*^{RNAi}*/+;* right) with
1224 probes targeting the indicated transcripts, showing an additional *Ir75d* expressing
1225 neuron in ac4. Bottom quadrants show higher magnification of a single Z-slice. Scale
1226 bars, 25 µm, or 3 µm for quadrants.
1227 **(J)** Schematic of the inferred states of ac4 sensilla in control, *mamo*^{RNAi} and PCD-
1228 blocked antennae.
1229
1230 **Figure 7. *Slp2* activity is necessary and sufficient to specify PCD in the at1**
1231 **lineage.**
1232 **(A)** Volcano plot illustrating differentially-expressed genes between at1 undead and
1233 Or67d OSN populations (pseudobulk analysis, *x* axis = $\log_2$FC("undead"/control), *y*
1234 axis = -$\log_{10}$(adjusted P), $\log_2$FC > 0.25, % of positive nuclei > 0.25). Pro-apoptotic
1235 genes are highlighted in blue, and TFs whose expression is enriched in the undead
1236 at1 neurons are highlighted in red.
1237 **(B)** UMAPs of the at1 lineage (integrated control and PCD-blocked conditions),
1238 illustrating neuron identity and *slp2* expression.
1239 **(C)** Traces of spontaneous (top) and cVA-evoked (bottom) electrophysiological
1240 activity from the at1 sensillum in the antennae of control (*peb-Gal4,UAS-Dcr-2*),
1241 PCD-blocked (*peb-Gal4/+;UAS-p35/+;*) and *slp2*^{RNAi} (*peb-Gal4,UAS-Dcr-2/+;;UAS-*
1242 *slp2*^{RNAi}*/+*) animals. Red and blue arrows indicate spikes of the Or67d and undead
1243 neurons, respectively.
1244 **(D)** Quantification of the proportion of at1 sensilla housing 1 or >1 spike amplitude in
1245 the indicated genotypes (*n* is indicated above).
1246 **(E)** Schematic of the inferred states of the at1 sensillum in control and *slp2*^{RNAi}
1247 antennae.
1248 **(F)** RNA FISH experiment on whole-mount antennae of control animals (;;*UAS-slp2-*
1249 *ORF-3HA/+* and ;;*at1-Gal4/+*) and in animals over-expressing *slp2* specifically and
1250 transiently in the at1 lineage during development (Chai et al., 2019) (;;*UAS-slp2-*
1251 *ORF-3HA/at1-Gal4*) with probes targeting *Or67d*. Scale bar, 25 µm.

bioRxiv preprint doi: https://doi.org/10.1101/2025.01.16.632932; this version posted January 16, 2025. The copyright holder for this preprint (which was not certified by peer review) is the author/funder, who has granted bioRxiv a license to display the preprint in perpetuity. It is made available under aCC-BY-ND 4.0 International license.

1252 **(G)** Quantification of Or67d neurons in the indicated genotypes (*n* is indicated
1253 underneath). A and B letters indicate significant differences: P < 0.05 in pairwise
1254 comparisons (Wilcoxon rank sum test followed by Bonferroni correction for multiple
1255 comparisons).
1256
1257 **Figure 8. Context-specific requirement for Slp2 in PCD.**
1258 **(A)** Dot plot showing the expression of *slp2* in all annotated neuron lineages
1259 described in this work (control and PCD-blocked integrated datasets).
1260 **(B)** RNA FISH on whole-mount antennae of control (*peb-Gal4,UAS-Dcr-2*, top row)
1261 and *slp2*^{RNAi} animals (*peb-Gal4,UAS-Dcr-2/+;;UAS-slp2*^{RNAi}/+, bottom row) with
1262 probes targeting the indicated transcripts. Scale bar, 25 µm.xrele
1263 **(C)** Quantification of neurons from (B). *n* is indicated below each condition. * and ns
1264 indicate P < 0.05 and P > 0.05, respectively, *t* test.
1265 **(D)** RNA FISH on whole-mount antennae of control (*peb-Gal4,UAS-Dcr-2*, top row)
1266 and *slp2*^{RNAi} animals (*peb-Gal4,UAS-Dcr-2/+;;UAS-slp2*^{RNAi}/+, bottom row) with
1267 probes targeting the indicated transcripts. Scale bar, 25 µm.
1268 **(E)** Quantification of neurons from (D). *n* is indicated below each condition.
1269 **(F)** Schematic of inferred states of the ab10 sensillum in control and *slp2*^{RNAi}
1270 antennae.
1271 **(G)** RNA FISH on whole-mount antennae of control (*peb-Gal4,UAS-Dcr-2*, top row)
1272 and *slp2*^{RNAi} animals (*peb-Gal4,UAS-Dcr-2/+;;UAS-slp2*^{RNAi}/+, bottom row) with
1273 probes targeting the indicated transcripts. Scale bar, 25 µm.
1274 **(H)** Quantification of neurons from (G). *n* is indicated below each condition.
1275 **(I)** Schematic of inferred states of the at4 sensillum in control and *slp2*^{RNAi} antennae.
1276 **(J)** RNA FISH on whole-mount antennae of control (*peb-Gal4,UAS-Dcr-2*, top row)
1277 and *slp2*^{RNAi} animals (*peb-Gal4,UAS-Dcr-2/+;;UAS-slp2*^{RNAi}/+, bottom row) with
1278 probes targeting the indicated transcripts. Scale bar, 25 µm.
1279 **(K)** Quantification of neurons from (G). *n* is indicated below each condition.
1280 **(L)** Schematic of inferred states of the at4 sensillum in the antennae of widely used
1281 *Drosophila melanogaster* strains. The number of "+" sign reflects the relative
1282 prevalence of at4 subtypes (- = absent).
1283 **(E,H,K)** A-D letters indicate significant differences: P < 0.05 in pairwise comparisons
1284 (Wilcoxon rank sum test followed by Bonferroni correction for multiple comparisons).
1285
1286

bioRxiv preprint doi: https://doi.org/10.1101/2025.01.16.632932; this version posted January 16, 2025. The copyright holder for this preprint (which was not certified by peer review) is the author/funder, who has granted bioRxiv a license to display the preprint in perpetuity. It is made available under aCC-BY-ND 4.0 International license.

1287 **Supplementary Figures**
1288
1289 **Figure S1. Global cell type annotation of the developing antenna.**
1290 **(A)** Distribution of the number of genes detected per nucleus across all sequenced
1291 nuclei in control and PCD-blocked datasets. The dashed vertical lines indicate the
1292 mean.
1293 **(B)** UMAPs illustrating the unsupervised clustering of all nuclei from the integrated
1294 control and PCD-blocked datasets (top left), cell type scoring using marker gene
1295 modules extracted from the Fly Cell Atlas (Li et al., 2022) (see Methods), and cell
1296 type annotation of the integrated datasets (bottom right). Nuclei from clusters 15 and
1297 26 were sparse and exhibited a mixed identity; we therefore assigned these as
1298 doublets and discarded them from downstream analyses.
1299 **(C)** Expression score of cell type marker gene modules and the fraction of detected
1300 mitochondrial genes in each cluster.
1301 **(D)** Cell type and nuclei number composing the integrated, control and PCD-blocked
1302 datasets.
1303
1304 **Figure S2. Hallmarks of peripheral olfactory system development.**
1305 **(A)** Expression score of early, mid and late developmental time marker gene modules
1306 in early, mid and late olfactory, hygrosensory and thermosensory neurons, integrated
1307 datasets. Boxes show the median (thick line), first and third quartiles, while whiskers
1308 indicate data distribution limits. A-C letters indicate significant differences: $P < 0.05$ in
1309 pairwise comparisons (Wilcoxon rank sum test followed by Bonferroni correction for
1310 multiple comparisons).
1311 **(B)** Expression of the top 30 genes ($\log_2$FC) of each developmental time marker
1312 module in neurons grouped by developmental time (integrated datasets).
1313 **(C)** Gene Ontology (GO) analysis illustrating the top 10 ($\log_{10}$(adjusted P)) Biological
1314 Process (BP), Molecular Function (MF) and Cellular Component (CC) categories
1315 enriched in early, mid and late developmental marker gene modules (810 genes
1316 total).
1317
1318 **Figure S3. Initial annotation of neuronal subclusters based upon sensory**
1319 **receptor expression.**
1320 **(A)** UMAPs of unsupervised clustering of the sensory neurons (integrated datasets)
1321 at iteration 0 (left) and the initial annotation of a subset of these (typically late-stage
1322 cells) based upon sensory receptor gene expression in the control dataset (right).
1323 **(B)** Expression of diagnostic *Or* and *Ir* genes (and the glial marker *repo*) in each
1324 cluster from (A) (left UMAP, control dataset only).
1325 **(C)** UMAPs of unsupervised sub-clustering of the multiple_OR cluster from (A) (right
1326 UMAP) (top) and the annotation based upon sensory receptor gene expression in the
1327 control dataset (bottom).
1328 **(D)** Expression of diagnostic *Or* and *Ir* genes in each cluster in (C) (top UMAP;
1329 control dataset only).
1330
1331 **Figure S4. Backward, iterative annotation of subclusters based upon sensory**
1332 **receptor expression.**
1333 **(A)** UMAPs at iteration 0 of sensory neurons annotation (left) and highlighting at4
1334 neurons Or88a (red), Or65a/b/c (green) and Or47b (blue) (right).
1335 **(B)** Ranked expression score (left-to-right) of each at4 OSN marker gene module
1336 extracted from the iteration 0 annotated dataset. The top 5 unannotated clusters with

bioRxiv preprint doi: https://doi.org/10.1101/2025.01.16.632932; this version posted January 16, 2025. The copyright holder for this preprint (which was not certified by peer review) is the author/funder, who has granted bioRxiv a license to display the preprint in perpetuity. It is made available under aCC-BY-ND 4.0 International license.

1337 the highest scores for each OSN population marker genes modules are shown,
1338 allowing us to assign clusters from earlier developmental stage (typically lacking
1339 sensory receptor expression) to each at4 OSN, as indicated in the text on the right.
1340 These clusters were used for a subsequent round of marker gene scoring.
1341 **(C)** UMAPs at iteration 1 of sensory neurons annotation (left) and highlighting Or88a
1342 (red), Or65a/b/c (green) and Or47b (blue) neurons (right).
1343 **(D)** Ranked expression score (left-to-right) of each at4 OSN marker gene module
1344 extracted from the iteration 1 annotated object. The top 5 unannotated clusters with
1345 the highest scores for each OSN population marker genes modules are shown,
1346 allowing us to assign clusters to Or88a but not Or47b or Or65a/b/c OSNs, as
1347 indicated in the text on the right). These clusters were used for a subsequent round
1348 of marker gene scoring.
1349 **(E)** UMAPs at iteration 2 of sensory neurons (left) and highlighting Or88a (red),
1350 Or65/a/b/c (green) and Or47b (blue) neurons (right). No further sensory neuron
1351 lineage-based backward annotation was possible.
1352 **(F)** UMAP at iteration 2 (as in (E)) with sensilla-based annotations.
1353 **(G)** Ranked expression score (left-to-right) of the at4 sensillum marker gene module
1354 extracted from the iteration 2, sensilla based, annotated object. The top 5
1355 unannotated clusters with the highest scores are shown, allowing us to assign
1356 clusters to at4, as indicated in the text on the right. These clusters were used for a
1357 subsequent round of marker gene scoring.
1358 **(H)** UMAPs at iteration 3 of the sensilla-based annotation of sensory neurons (left)
1359 and highlighting the at4 sensillum (right).
1360
1361 **Figure S5. Sensory neuron type marker genes.**
1362 **(A)** GO analysis illustrating the top 25 ($\log_{10}$(adjusted P)) Biological Process (BP),
1363 Molecular Function (MF) and Cellular Component (CC) categories enriched in OSNs
1364 marker gene modules (1242 genes total). Only the control dataset was analyzed in
1365 this and the following panel.
1366 **(B)** Expression of OSN marker genes belonging to the indicated GO categories.
1367
1368 **Figure S6. Sensilla marker genes.**
1369 **(A)** Expression score of sensilla marker gene modules across sensilla (control
1370 dataset only in this and other panels).
1371 **(B)** Gene Ontology (GO) analysis illustrating the top 25 ($\log_{10}$(adjusted P)) Biological
1372 Process (BP), Molecular Function (MF) and Cellular Component (CC) categories
1373 enriched in sensilla marker gene modules (727 genes total).
1374 **(C)** Expression of sensilla marker genes belonging to GO:0003700.
1375 **(D)** Expression of the top 5 marker genes ($\log_2$FC) of each sensillum class.
1376
1377 **Figure S7. Sensory neuron precursor type marker genes.**
1378 **(A)** Expression score of Naa, Nab, Nba and Nbb marker gene modules in each
1379 sensory neuron precursor type category. Boxes show the median (thick line), first and
1380 third quartiles, while whiskers indicate data distribution limits. A-D letters indicate
1381 significant differences: $P < 0.05$ in pairwise comparisons (Wilcoxon rank sum test
1382 followed by Bonferroni correction for multiple comparisons). Only the control dataset
1383 was analyzed in this and the following panels.
1384 **(B)** Expression of the top 20 genes ($\log_2$FC) from each of the sensory neuron
1385 precursor type marker gene modules across sensory neuron precursor types.

bioRxiv preprint doi: https://doi.org/10.1101/2025.01.16.632932; this version posted January 16, 2025. The copyright holder for this preprint (which was not certified by peer review) is the author/funder, who has granted bioRxiv a license to display the preprint in perpetuity. It is made available under aCC-BY-ND 4.0 International license.

1386 **(C)** Gene Ontology (GO) analysis showing the top 25 (log_{10}(adjusted P)) Biological
1387 Process (BP), Molecular Function (MF) and Cellular Component (CC) categories
1388 enriched in OSN type marker gene modules (200 genes total).
1389 **(D)** Expression of sensory neuron precursor type marker genes belonging to
1390 GO:0007411.
1391 **(E-F)** UMAPs of ac1 (E) and at4 (F) with annotation and developmental phases (top
1392 left), the expression of diagnostic sensory receptors (top right), the expression score
1393 of sensory neuron precursor type marker gene modules (bottom left) and a schematic
1394 illustrating the inferred precursor type and identity of sensory neurons (bottom right).
1395 A-D letters indicate significant differences: $P < 0.05$ in pairwise comparisons
1396 (Wilcoxon rank sum test followed by Bonferroni correction for multiple comparisons).
1397
1398 **Figure S8. Putative transcription factor codes underlying sensory neuron**
1399 **identity.**
1400 Differentially expressed TFs in sensory neuron populations (control dataset). TFs
1401 functionally characterized in this work are highlighted.
1402
1403 **Figure S9. Sensory receptor expression during antennal development.**
1404 Expression of tuning and co-receptor subunits across cell types from different
1405 developmental phases (control dataset).
1406
1407 **Figure S10. Examples of receptor co-expression.**
1408 **(A)** Top: UMAPs of the sacIII_v/d-Amt lineage (control dataset) illustrating the
1409 developmental stages and receptor expression patterns; *Rh50* encodes an ammonia
1410 transporter that is co-expressed with Amt in these ammonia-sensing neurons
1411 although its role is unclear (Vulpe et al., 2021). Bottom: a pseudotime UMAP and
1412 corresponding receptor expression dynamics.
1413 **(B)** Left: RNA FISH on whole-mount antennae of control (*peb-Gal4*) animals with
1414 probes targeting the indicated transcripts (n = 10-12). The ac3 and ac1 sensilla
1415 zones are indicated. Bottom row shows a higher magnification of sacIII-v/d-Amt
1416 neurons co-expressing *Amt* and *Or35a* in 3 adjacent confocal Z-slices. Scale bars, 25
1417 µm (top images) or 10 µm (bottom images). Right: schematic of olfactory (co)-
1418 receptor subunits expressed in sacIII-v/d-Amt neurons.
1419 **(C-E)** Top: UMAPs of the ac1-Ir31a (C), ab5B-Or47a/Or33b (D) and ab8B-Or9a (E)
1420 lineages (control dataset) illustrating the developmental stages and receptor
1421 expression patterns. Bottom: pseudotime UMAPs and corresponding receptor
1422 expression dynamics.
1423
1424 **Figure S11. Global survey of chemosensory receptor expression in late stages.**
1425 Expression of all detected sensory receptor subunits in the late developmental phase
1426 (control dataset).
1427
1428 **Figure S12. Expression of pro-apoptotic genes.**
1429 **(A)** UMAPs illustrating the expression of the pro-apoptotic genes *reaper* (*rpr*), *grim*,
1430 *sickle* (*skl*) and *head involution defective* (*hid)* genes in annotated nuclei of control
1431 and PCD-blocked datasets.
1432 **(B)** Average expression (left) and fraction of positive nuclei (right) for these genes in
1433 control and PCD-blocked datasets.
1434 **(C)** Abundance of each neuronal class in control (top) and PCD-blocked (middle)
1435 datasets, calculated as the percentage of nuclei for each class relative to the total

bioRxiv preprint doi: https://doi.org/10.1101/2025.01.16.632932; this version posted January 16, 2025. The copyright holder for this preprint (which was not certified by peer review) is the author/funder, who has granted bioRxiv a license to display the preprint in perpetuity. It is made available under aCC-BY-ND 4.0 International license.

1436 number of nuclei (from 36 h APF, excluding those forming new clusters in the PCD-
1437 blocked dataset) and fold-change in the abundance of each class in the PCD-blocked
1438 dataset relative to the control dataset (bottom).
1439
1440 **Figure S13. Expression of co-receptors in undead neurons.**
1441 **(A)** UMAPs of the integrated ac3I/II dataset illustrating the expression of tuning
1442 receptors (as in Figure 5D) and co-receptors in endogenous and undead neurons.
1443 **(B)** UMAPs of the integrated sacIII-v/d dataset illustrating the expression of tuning
1444 receptors (as in Figure 5K) and co-receptors in endogenous and undead neurons.
1445
1446 **Figure S14. Analysis of the undead neuron lineages in additional sensilla.**
1447 **(A)** UMAPs of the ab10 lineage from control and PCD-blocked datasets illustrating
1448 the developmental stages (top) and RGS expression (bottom), revealing that some
1449 cells with high RGS score are present exclusively in PCD-blocked animals.
1450 **(B)** Lineage annotation of the ab10 sensillum in control and PCD-blocked integrated
1451 datasets (top), ranked RGS score (left-to-right) (bottom left) and precursor type score
1452 (bottom right) for each OSN type in the integrated datasets. Boxes show the median
1453 (thick line), first and third quartiles, while whiskers indicate data distribution limits,
1454 here and elsewhere.
1455 **(C)** Expression of the indicated receptor in the integrated control and PCD-blocked
1456 datasets. No receptor was robustly detected in the undead neuron population.
1457 **(D)** Schematic of the inferred states of the ab10 sensillum in control and PCD-
1458 blocked antennae.
1459 **(E)** UMAPs of the ab5 lineage from control and PCD-blocked datasets illustrating the
1460 developmental stages (top) and RGS expression (bottom), revealing that some cells
1461 with high RGS score are present exclusively in PCD-blocked animals.
1462 **(F)** Lineage annotation of the ab5 sensillum in control and PCD-blocked integrated
1463 datasets (top), ranked RGS score (left-to-right) (bottom left) and precursor type score
1464 (bottom right) for each OSN type in the integrated datasets.
1465 **(G)** Expression of the indicated receptor in the integrated control and PCD-blocked
1466 datasets. No receptor was robustly detected in the undead neuron population.
1467 **(H)** Schematic of the inferred states of the ab5 sensillum in control and PCD-blocked
1468 antennae.
1469 **(I)** UMAPs of the sacI lineage from control and PCD-blocked datasets illustrating the
1470 developmental stages (top) and RGS expression (bottom), revealing that some cells
1471 with high RGS score are present exclusively in PCD-blocked animals.
1472 **(J)** Lineage annotation of the sacI sensillum in control and PCD-blocked integrated
1473 datasets (top), ranked RGS score (left-to-right) (bottom left) and precursor type score
1474 (bottom right) for each OSN type in the integrated datasets.
1475 **(K)** Expression of the indicated receptor in the integrated control and PCD-blocked
1476 datasets. No receptor was robustly detected in the undead neuron population.
1477 **(L)** Schematic of the inferred states of the sacI sensillum in control and PCD-blocked
1478 antennae.
1479 **(M-N)** UMAPs of the ai3 (E) and ab4 (F) lineages from control and PCD-blocked
1480 datasets illustrating the developmental stages (top) and RGS expression (bottom).
1481 No undead neurons were apparent.
1482 **(B,F,J)** A-D letters indicate significant differences: $P < 0.05$ in pairwise comparisons
1483 (Wilcoxon rank sum test followed by Bonferroni correction for multiple comparisons).
1484
1485

bioRxiv preprint doi: https://doi.org/10.1101/2025.01.16.632932; this version posted January 16, 2025. The copyright holder for this preprint (which was not certified by peer review) is the author/funder, who has granted bioRxiv a license to display the preprint in perpetuity. It is made available under aCC-BY-ND 4.0 International license.

1486 **Figure S15. Analysis of Ir75d neuron projection patterns.**
1487 **(A)** *Ir75b/c* RNA FISH and anti-GFP immunofluorescence on whole-mount antennae
1488 of control (*peb-Gal4/+;Ir75d-CD4-GFP/+*; top), *mamo*^{RNAi} (*peb-Gal4,UAS-Dcr-*
1489 *2/+;UAS-mamo*^{RNAi}*/Ir75d-CD4-GFP;* middle) and PCD-blocked (*peb-Gal4/+;UAS-*
1490 *p35/Ir75d-CD4-GFP;* bottom) animals (*n* = 10, 11 and 6, respectively). Scale bars, 25
1491 µm.
1492 **(B)** GFP and nc82 immunofluorescence on whole-mount brains of control (*peb-*
1493 *Gal4/+;Ir75d-CD4-GFP/+;* top), *mamo*^{RNAi} (*peb-Gal4,UAS-Dcr-2/+;UAS-*
1494 *mamo*^{RNAi}*/Ir75d-CD4-GFP*; middle) and PCD-blocked (*peb-Gal4/+;UAS-p35/Ir75d-*
1495 *CD4-GFP;* bottom) animals (*n* = 4, 8 and 6, respectively). Scale bars, 25 µm.
1496
1497

bioRxiv preprint doi: https://doi.org/10.1101/2025.01.16.632932; this version posted January 16, 2025. The copyright holder for this preprint (which was not certified by peer review) is the author/funder, who has granted bioRxiv a license to display the preprint in perpetuity. It is made available under aCC-BY-ND 4.0 International license.

1498 **References**
1499

1500 Abuin, L., Bargeton, B., Ulbrich, M.H., Isacoff, E.Y., Kellenberger, S., and Benton, R.
1501 (2011). Functional architecture of olfactory ionotropic glutamate receptors. Neuron
1502 *69*, 44-60.
1503 Auer, T.O., Alvarez-Ocana, R., Cruchet, S., Benton, R., and Arguello, J.R. (2022).
1504 Copy number changes in co-expressed odorant receptor genes enable selection for
1505 sensory differences in drosophilid species. Nature ecology & evolution *6*, 1343-1353.
1506 Auer, T.O., Khallaf, M.A., Silbering, A.F., Zappia, G., Ellis, K., Alvarez-Ocana, R.,
1507 Arguello, J.R., Hansson, B.S., Jefferis, G.S.X.E., Caron, S.J.C.*, et al.* (2020).
1508 Olfactory receptor and circuit evolution promote host specialization. Nature *579*, 402-
1509 408.
1510 Barish, S., and Volkan, P.C. (2015). Mechanisms of olfactory receptor neuron
1511 specification in *Drosophila*. Wiley interdisciplinary reviews Developmental biology *4*,
1512 609-621.
1513 Benton, R. (2022). *Drosophila* olfaction: past, present and future. Proc Biol Sci *289*,
1514 20222054.
1515 Benton, R., and Dahanukar, A. (2023). Recording from Fly Olfactory Sensilla. Cold
1516 Spring Harb Protoc *2023*, pdb prot108063.
1517 Benton, R., Mermet, J., Jang, A., Endo, K., Cruchet, S., and Menuz, K. (2025). An
1518 integrated anatomical, functional and evolutionary view of the *Drosophila* olfactory
1519 system. bioRxiv.
1520 Benton, R., Sachse, S., Michnick, S.W., and Vosshall, L.B. (2006). Atypical
1521 membrane topology and heteromeric function of *Drosophila* odorant receptors *in vivo*.
1522 PLOS Biol *4*, e20.
1523 Benton, R., Vannice, K.S., Gomez-Diaz, C., and Vosshall, L.B. (2009). Variant
1524 ionotropic glutamate receptors as chemosensory receptors in *Drosophila*. Cell *136*,
1525 149-162.
1526 Benton, R., Vannice, K.S., and Vosshall, L.B. (2007). An essential role for a CD36-
1527 related receptor in pheromone detection in *Drosophila*. Nature *450*, 289-293.
1528 Bontonou, G., Saint-Leandre, B., Kafle, T., Baticle, T., Hassan, A., Sanchez-Alcaniz,
1529 J.A., and Arguello, J.R. (2024). Evolution of chemosensory tissues and cells across
1530 ecologically diverse Drosophilids. Nat Commun *15*, 1047.
1531 Cao, J., Spielmann, M., Qiu, X., Huang, X., Ibrahim, D.M., Hill, A.J., Zhang, F.,
1532 Mundlos, S., Christiansen, L., Steemers, F.J.*, et al.* (2019). The single-cell
1533 transcriptional landscape of mammalian organogenesis. Nature *566*, 496-502.
1534 Chai, P.C., Cruchet, S., Wigger, L., and Benton, R. (2019). Sensory neuron lineage
1535 mapping and manipulation in the *Drosophila* olfactory system. Nat Commun *10*, 643.
1536 Corthals, K., Andersson, V., Churcher, A., Reimegard, J., and Enjin, A. (2023).
1537 Genetic atlas of hygro-and thermosensory cells in the vinegar fly *Drosophila*
1538 *melanogaster*. Sci Rep *13*, 15202.
1539 Couto, A., Alenius, M., and Dickson, B.J. (2005). Molecular, anatomical, and
1540 functional organization of the *Drosophila* olfactory system. Curr Biol *15*, 1535-1547.
1541 Croset, V., Rytz, R., Cummins, S.F., Budd, A., Brawand, D., Kaessmann, H., Gibson,
1542 T.J., and Benton, R. (2010). Ancient protostome origin of chemosensory ionotropic
1543 glutamate receptors and the evolution of insect taste and olfaction. PLOS Genet *6*,
1544 e1001064.
1545 Davie, K., Janssens, J., Koldere, D., De Waegeneer, M., Pech, U., Kreft, L., Aibar, S.,
1546 Makhzami, S., Christiaens, V., Bravo Gonzalez-Blas, C.*, et al.* (2018). A Single-Cell
1547 Transcriptome Atlas of the Aging *Drosophila* Brain. Cell *174*, 982-998 e920.

bioRxiv preprint doi: https://doi.org/10.1101/2025.01.16.632932; this version posted January 16, 2025. The copyright holder for this preprint (which was not certified by peer review) is the author/funder, who has granted bioRxiv a license to display the preprint in perpetuity. It is made available under aCC-BY-ND 4.0 International license.

1548 de Bruyne, M., Foster, K., and Carlson, J.R. (2001). Odor coding in the *Drosophila*
1549 antenna. Neuron *30*, 537-552.
1550 Endo, K., Aoki, T., Yoda, Y., Kimura, K., and Hama, C. (2007). Notch signal
1551 organizes the *Drosophila* olfactory circuitry by diversifying the sensory neuronal
1552 lineages. Nat Neurosci *10*, 153-160.
1553 Endo, K., Karim, M.R., Taniguchi, H., Krejci, A., Kinameri, E., Siebert, M., Ito, K.,
1554 Bray, S.J., and Moore, A.W. (2011). Chromatin modification of Notch targets in
1555 olfactory receptor neuron diversification. Nature Neuroscience *15*, 224-233.
1556 Fishilevich, E., and Vosshall, L.B. (2005). Genetic and functional subdivision of the
1557 *Drosophila* antennal lobe. Curr Biol *15*, 1548-1553.
1558 Fujii, S., Yavuz, A., Slone, J., Jagge, C., Song, X., and Amrein, H. (2015). *Drosophila*
1559 Sugar Receptors in Sweet Taste Perception, Olfaction, and Internal Nutrient Sensing.
1560 Curr Biol *25*, 621-627.
1561 Grabe, V., Baschwitz, A., Dweck, H.K.M., Lavista-Llanos, S., Hansson, B.S., and
1562 Sachse, S. (2016). Elucidating the Neuronal Architecture of Olfactory Glomeruli in the
1563 *Drosophila* Antennal Lobe. Cell Rep *16*, 3401-3413.
1564 Grosjean, Y., Rytz, R., Farine, J.P., Abuin, L., Cortot, J., Jefferis, G.S., and Benton,
1565 R. (2011). An olfactory receptor for food-derived odours promotes male courtship in
1566 *Drosophila*. Nature *478*, 236-240.
1567 Hafemeister, C., and Satija, R. (2019). Normalization and variance stabilization of
1568 single-cell RNA-seq data using regularized negative binomial regression. Genome
1569 Biol *20*, 296.
1570 Hansson, B.S., and Stensmyr, M.C. (2011). Evolution of insect olfaction. Neuron *72*,
1571 698-711.
1572 Henry, G.L., Davis, F.P., Picard, S., and Eddy, S.R. (2012). Cell type-specific
1573 genomics of *Drosophila* neurons. Nucleic Acids Res *40*, 9691-9704.
1574 Jafari, S., Alkhori, L., Schleiffer, A., Brochtrup, A., Hummel, T., and Alenius, M.
1575 (2012). Combinatorial activation and repression by seven transcription factors specify
1576 *Drosophila* odorant receptor expression. PLOS Biology *10*, e1001280.
1577 Jefferis, G.S., and Hummel, T. (2006). Wiring specificity in the olfactory system.
1578 Semin Cell Dev Biol *17*, 50-65.
1579 Jones, W.D., Cayirlioglu, P., Grunwald Kadow, I., and Vosshall, L.B. (2007). Two
1580 chemosensory receptors together mediate carbon dioxide detection in *Drosophila*.
1581 Nature *445*, 86-90.
1582 Junion, G., Bataille, L., Jagla, T., Da Ponte, J.P., Tapin, R., and Jagla, K. (2007).
1583 Genome-wide view of cell fate specification: ladybird acts at multiple levels during
1584 diversification of muscle and heart precursors. Genes Dev *21*, 3163-3180.
1585 Konstantinides, N., Holguera, I., Rossi, A.M., Escobar, A., Dudragne, L., Chen, Y.C.,
1586 Tran, T.N., Martinez Jaimes, A.M., Ozel, M.N., Simon, F., *et al.* (2022). A complete
1587 temporal transcription factor series in the fly visual system. Nature *604*, 316-322.
1588 Kumar, A., Tauxe, G.M., Perry, S., Scott, C.A., Dahanukar, A., and Ray, A. (2020).
1589 Contributions of the Conserved Insect Carbon Dioxide Receptor Subunits to Odor
1590 Detection. Cell Rep *31*, 107510.
1591 Kurtovic, A., Widmer, A., and Dickson, B.J. (2007). A single class of olfactory
1592 neurons mediates behavioural responses to a *Drosophila* sex pheromone. Nature
1593 *446*, 542-546.
1594 Kwon, J.Y., Dahanukar, A., Weiss, L.A., and Carlson, J.R. (2007). The molecular
1595 basis of CO_2 reception in *Drosophila*. Proceedings of the National Academy of
1596 Sciences of the United States of America *104*, 3574-3578.

bioRxiv preprint doi: https://doi.org/10.1101/2025.01.16.632932; this version posted January 16, 2025. The copyright holder for this preprint (which was not certified by peer review) is the author/funder, who has granted bioRxiv a license to display the preprint in perpetuity. It is made available under aCC-BY-ND 4.0 International license.

1597 Levine, J.H., Simonds, E.F., Bendall, S.C., Davis, K.L., Amir el, A.D., Tadmor, M.D.,
1598 Litvin, O., Fienberg, H.G., Jager, A., Zunder, E.R., *et al.* (2015). Data-Driven
1599 Phenotypic Dissection of AML Reveals Progenitor-like Cells that Correlate with
1600 Prognosis. Cell *162*, 184-197.
1601 Li, H., Janssens, J., De Waegeneer, M., Kolluru, S.S., Davie, K., Gardeux, V.,
1602 Saelens, W., David, F.P.A., Brbic, M., Spanier, K., *et al.* (2022). Fly Cell Atlas: A
1603 single-nucleus transcriptomic atlas of the adult fruit fly. Science *375*, eabk2432.
1604 Li, H., Li, T., Horns, F., Li, J., Xie, Q., Xu, C., Wu, B., Kebschull, J.M., McLaughlin,
1605 C.N., Kolluru, S.S., *et al.* (2020). Single-Cell Transcriptomes Reveal Diverse
1606 Regulatory Strategies for Olfactory Receptor Expression and Axon Targeting. Curr
1607 Biol *30*, 1189-1198 e1185.
1608 Liu, L.Y., Long, X., Yang, C.P., Miyares, R.L., Sugino, K., Singer, R.H., and Lee, T.
1609 (2019). Mamo decodes hierarchical temporal gradients into terminal neuronal fate.
1610 Elife *8*, e48056.
1611 McLaughlin, C.N., Brbic, M., Xie, Q., Li, T., Horns, F., Kolluru, S.S., Kebschull, J.M.,
1612 Vacek, D., Xie, A., Li, J., *et al.* (2021). Single-cell transcriptomes of developing and
1613 adult olfactory receptor neurons in *Drosophila*. Elife *10*, e63856.
1614 Menuz, K., Larter, N.K., Park, J., and Carlson, J.R. (2014). An RNA-Seq Screen of
1615 the *Drosophila* Antenna Identifies a Transporter Necessary for Ammonia Detection.
1616 PLOS Genet *10*, e1004810.
1617 Mika, K., and Benton, R. (2021). Olfactory Receptor Gene Regulation in Insects:
1618 Multiple Mechanisms for Singular Expression. Frontiers in neuroscience *15*, 738088.
1619 Mika, K., Cruchet, S., Chai, P.C., Prieto-Godino, L.L., Auer, T.O., Pradervand, S.,
1620 and Benton, R. (2021). Olfactory receptor-dependent receptor repression in
1621 *Drosophila*. Science advances *7*, eabe3745.
1622 Munch, D., and Galizia, C.G. (2016). DoOR 2.0--Comprehensive Mapping of
1623 *Drosophila melanogaster* Odorant Responses. Sci Rep *6*, 21841.
1624 Nava Gonzales, C., McKaughan, Q., Bushong, E.A., Cauwenberghs, K., Ng, R.,
1625 Madany, M., Ellisman, M.H., and Su, C.Y. (2021). Systematic morphological and
1626 morphometric analysis of identified olfactory receptor neurons in *Drosophila*
1627 *melanogaster*. Elife *10*, e69896.
1628 Pal Mahadevan, V., Lavista-Llanos, S., Knaden, M., and Hansson, B.S. (2022). No
1629 functional contribution of the gustatory receptor, Gr64b, co-expressed in olfactory
1630 sensory neurons of *Drosophila melanogaster*. Frontiers in Ecology and Evolution *10*.
1631 Pinto-Teixeira, F., Konstantinides, N., and Desplan, C. (2016). Programmed cell
1632 death acts at different stages of *Drosophila* neurodevelopment to shape the central
1633 nervous system. FEBS Lett *590*, 2435-2453.
1634 Prieto-Godino, L.L., Rytz, R., Cruchet, S., Bargeton, B., Abuin, L., Silbering, A.F.,
1635 Ruta, V., Dal Peraro, M., and Benton, R. (2017). Evolution of Acid-Sensing Olfactory
1636 Circuits in Drosophilids. Neuron *93*, 661-676.
1637 Prieto-Godino, L.L., Silbering, A.F., Khallaf, M.A., Cruchet, S., Bojkowska, K.,
1638 Pradervand, S., Hansson, B.S., Knaden, M., and Benton, R. (2020). Functional
1639 integration of "undead" neurons in the olfactory system. Science advances *6*,
1640 eaaz7238.
1641 Qiu, X., Mao, Q., Tang, Y., Wang, L., Chawla, R., Pliner, H.A., and Trapnell, C.
1642 (2017). Reversed graph embedding resolves complex single-cell trajectories. Nat
1643 Methods *14*, 979-982.
1644 Ramdya, P., and Benton, R. (2010). Evolving olfactory systems on the fly. Trends
1645 Genet *26*, 307-316.

bioRxiv preprint doi: https://doi.org/10.1101/2025.01.16.632932; this version posted January 16, 2025. The copyright holder for this preprint (which was not certified by peer review) is the author/funder, who has granted bioRxiv a license to display the preprint in perpetuity. It is made available under aCC-BY-ND 4.0 International license.

1646 Robertson, H.M., Warr, C.G., and Carlson, J.R. (2003). Molecular evolution of the
1647 insect chemoreceptor gene superfamily in *Drosophila melanogaster*. Proc Natl Acad
1648 Sci USA *100 Suppl 2*, 14537-14542.
1649 Rodrigues, V., and Hummel, T. (2008). Development of the *Drosophila* olfactory
1650 system. Adv Exp Med Biol *628*, 82-101.
1651 Saina, M., and Benton, R. (2013). Visualizing olfactory receptor expression and
1652 localization in *Drosophila*. Methods in Molecular Biology *1003*, 211-228.
1653 Schindelin, J., Arganda-Carreras, I., Frise, E., Kaynig, V., Longair, M., Pietzsch, T.,
1654 Preibisch, S., Rueden, C., Saalfeld, S., Schmid, B.*, et al.* (2012). Fiji: an open-source
1655 platform for biological-image analysis. Nat Methods *9*, 676-682.
1656 Schlegel, P., Bates, A.S., Sturner, T., Jagannathan, S.R., Drummond, N., Hsu, J.,
1657 Serratosa Capdevila, L., Javier, A., Marin, E.C., Barth-Maron, A.*, et al.* (2021).
1658 Information flow, cell types and stereotypy in a full olfactory connectome. Elife *10*,
1659 e66018.
1660 Schmidt, H.R., and Benton, R. (2020). Molecular mechanisms of olfactory detection
1661 in insects: beyond receptors. Open Biol *10*, 200252.
1662 Sen, A., Kuruvilla, D., Pinto, L., Sarin, A., and Rodrigues, V. (2004). Programmed cell
1663 death and context dependent activation of the EGF pathway regulate gliogenesis in
1664 the *Drosophila* olfactory system. Mech Dev *121*, 65-78.
1665 Sen, A., Shetty, C., Jhaveri, D., and Rodrigues, V. (2005). Distinct types of glial cells
1666 populate the *Drosophila* antenna. BMC Dev Biol *5*, 25.
1667 Shang, X., Talross, G.J.S., and Carlson, J.R. (2024). Exitron splicing of odor receptor
1668 genes in *Drosophila*. Proceedings of the National Academy of Sciences of the United
1669 States of America *121*, e2320277121.
1670 Silbering, A.F., Rytz, R., Grosjean, Y., Abuin, L., Ramdya, P., Jefferis, G.S., and
1671 Benton, R. (2011). Complementary Function and Integrated Wiring of the
1672 Evolutionarily Distinct *Drosophila* Olfactory Subsystems. The Journal of
1673 Neuroscience *31*, 13357-13375.
1674 Su, C.Y., Menuz, K., Reisert, J., and Carlson, J.R. (2012). Non-synaptic inhibition
1675 between grouped neurons in an olfactory circuit. Nature *492*, 66-71.
1676 Sweeney, L.B., Couto, A., Chou, Y.H., Berdnik, D., Dickson, B.J., Luo, L., and
1677 Komiyama, T. (2007). Temporal target restriction of olfactory receptor neurons by
1678 Semaphorin-1a/PlexinA-mediated axon-axon interactions. Neuron *53*, 185-200.
1679 Takagi, S., Sancer, G., Abuin, L., Stupski, S.D., Arguello, J.R., Prieto-Godino, L.,
1680 Stern, D.L., Cruchet, S., Alvarez-Ocana, R., Wienecke, C.F.R.*, et al.* (2024).
1681 Olfactory sensory neuron population expansions influence projection neuron
1682 adaptation and enhance odour tracking. Nature Comm *15*, 7041.
1683 Task, D., Lin, C.C., Vulpe, A., Afify, A., Ballou, S., Brbic, M., Schlegel, P., Raji, J.,
1684 Jefferis, G., Li, H.*, et al.* (2022). Chemoreceptor co-expression in *Drosophila*
1685 *melanogaster* olfactory neurons. Elife *11*, e72599.
1686 Trapnell, C., Cacchiarelli, D., Grimsby, J., Pokharel, P., Li, S., Morse, M., Lennon,
1687 N.J., Livak, K.J., Mikkelsen, T.S., and Rinn, J.L. (2014). The dynamics and regulators
1688 of cell fate decisions are revealed by pseudotemporal ordering of single cells. Nat
1689 Biotechnol *32*, 381-386.
1690 van der Goes van Naters, W., and Carlson, J.R. (2007). Receptors and neurons for
1691 fly odors in *Drosophila*. Curr Biol *17*, 606-612.
1692 Vosshall, L.B., and Stocker, R.F. (2007). Molecular Architecture of Smell and Taste in
1693 *Drosophila*. Annu Rev Neurosci *30*, 505-533.

bioRxiv preprint doi: https://doi.org/10.1101/2025.01.16.632932; this version posted January 16, 2025. The copyright holder for this preprint (which was not certified by peer review) is the author/funder, who has granted bioRxiv a license to display the preprint in perpetuity. It is made available under aCC-BY-ND 4.0 International license.

1694 Vulpe, A., Kim, H.S., Ballou, S., Wu, S.T., Grabe, V., Nava Gonzales, C., Liang, T.,
1695 Sachse, S., Jeanne, J.M., Su, C.Y.*, et al.* (2021). An ammonium transporter is a non-
1696 canonical olfactory receptor for ammonia. Curr Biol *31*, 3382-3390 e3387.
1697 Vulpe, A., and Menuz, K. (2021). Ir76b is a Co-receptor for Amine Responses in
1698 *Drosophila* Olfactory Neurons. Front Cell Neurosci *15*, 759238.
1699 Wu, T., Hu, E., Xu, S., Chen, M., Guo, P., Dai, Z., Feng, T., Zhou, L., Tang, W.,
1700 Zhan, L.*, et al.* (2021). clusterProfiler 4.0: A universal enrichment tool for interpreting
1701 omics data. Innovation (Camb) *2*, 100141.
1702 Yao, C.A., Ignell, R., and Carlson, J.R. (2005). Chemosensory coding by neurons in
1703 the coeloconic sensilla of the *Drosophila* antenna. J Neurosci *25*, 8359-8367.
1704 Young, M.D., and Behjati, S. (2020). SoupX removes ambient RNA contamination
1705 from droplet-based single-cell RNA sequencing data. Gigascience *9*.
1706 Zhang, Y., Tsang, T.K., Bushong, E.A., Chu, L.A., Chiang, A.S., Ellisman, M.H.,
1707 Reingruber, J., and Su, C.Y. (2019). Asymmetric ephaptic inhibition between
1708 compartmentalized olfactory receptor neurons. Nat Commun *10*, 1560.
1709 Zhao, Z., and McBride, C.S. (2020). Evolution of olfactory circuits in insects. J Comp
1710 Physiol A Neuroethol Sens Neural Behav Physiol *206*, 353-367.
1711 Zhu, H., Zhao, S.D., Ray, A., Zhang, Y., and Li, X. (2022). A comprehensive temporal
1712 patterning gene network in *Drosophila* medulla neuroblasts revealed by single-cell
1713 RNA sequencing. Nat Commun *13*, 1247.
1714

Mermet Figure 1

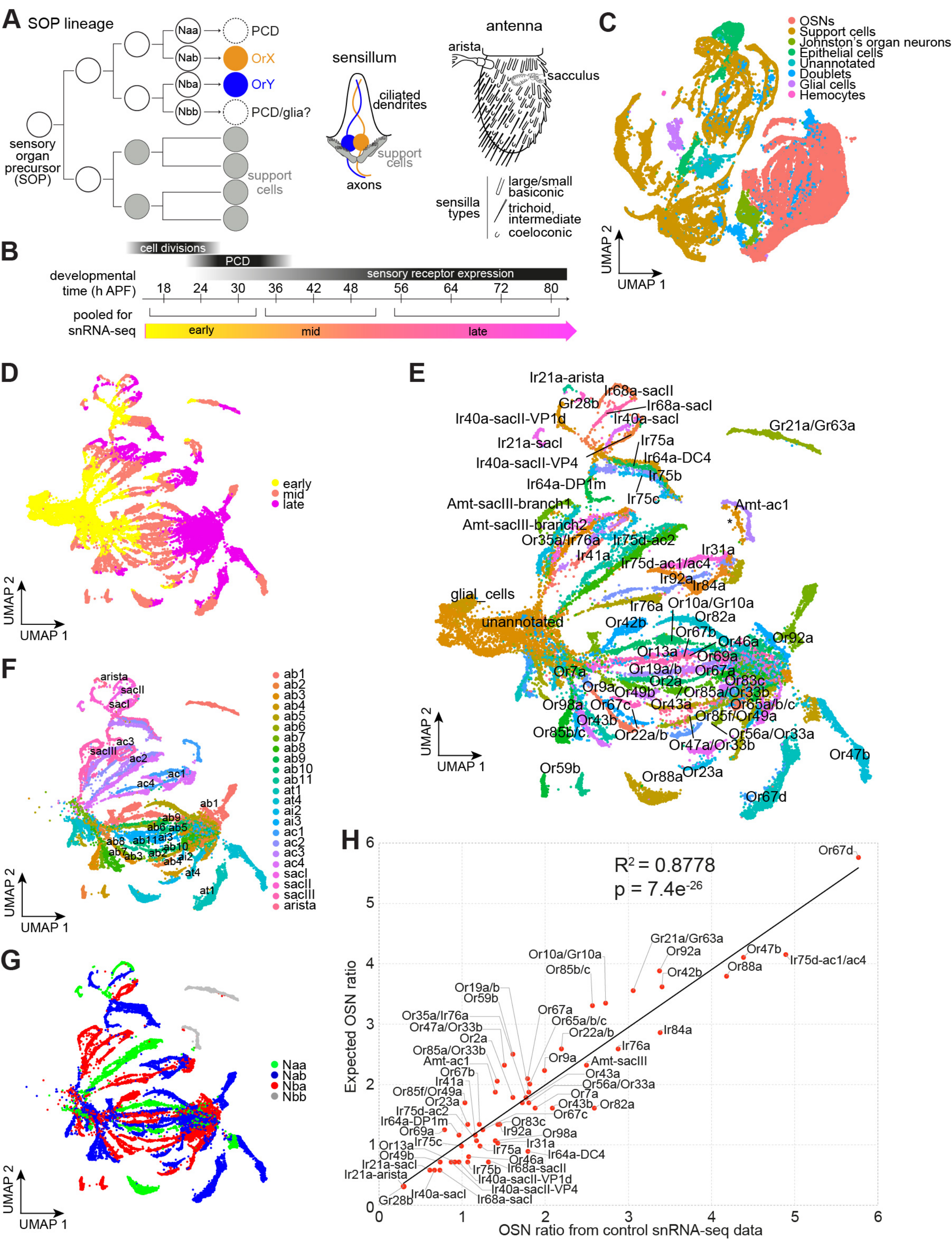

available under aCC-BY-ND 4.0 International license.

A
Percent expressed 0 20 40 60
Average expression 0 1 2
Cell type
Gr28b
Ir21a-arista
Amt-sacIII-branch2
Amt-sacIII-branch1
Ir64a-DP1m
Ir64a-DC4
Ir68a-sacII
Ir40a-sacII-VP4
Ir40a-sacII-VP1d
Ir21a-sacI
Ir68a-sacI
Ir40a-sacI
Ir75d-ac1/ac4
Ir76a
Ir84a
Ir75c
Ir75b
Or35a/Ir76a
Ir75d-ac2
Ir41a
Ir75a
Amt-ac1
Ir92a
Ir31a
Or2a
Or19a/b
Or43a
Or83c
Or23a
Or47b
Or88a
Or65a/b/c
Or67d
Or49b
Or67a
Or85f/Or49a
Or67b
Or69a
Or9a
Or43b
Or98a
Or67c
Or46a
Or13a
Or82a
Or47a/Or33b
Or7a
Or56a/Or33a
Or85b/c
Or22a/b
Or85a/Or33b
Or59b
Or10a/Gr10a
Or92a
Or42b
Gr21a/Gr63a
lz Or85f Or67a lbe lbl Or83c Or23a
Genes

B
ab10 lineage
Or67a Or85f
UMAP 1
UMAP 2
Or67a
Exp. level 2 1 0
Or85f
Exp. level 1 0.5 0
lz
Exp. level 2 1 0

C
Developmental phase
late
mid
early
lz Or85f Or67a
Genes
Percent expressed 0 20 40 60 80
Average expression 1 0 -1

D
ai2 lineage
Or83c Or23a
UMAP 1
UMAP 2
Or23a
Exp. level 1.5 1 0.5 0
Or83c
Exp. level 2 1 0
lbl
Exp. level 1.5 1 0.5 0
lbe
Exp. level 1 0.5 0

E
Developmental phase
late
mid
early
lbl lbe Or83c Or23a
Genes
Percent expressed 0 10 20 30 40 50
Average expression 1 0 -1

F
peb-Gal4
Or67a lz Merge
Or85f lz Merge

G
peb-Gal4>UAS-Dcr-2
peb-Gal4>UAS-Dcr-2, UAS-lz^{RNAi}
Or67a Or67a
Or85f Or85f

H
No. of neurons
Or67a *** Or85f *** Or67b ns
peb-Gal4> UAS-Dcr-2 + + + + + +
UAS-lz^{RNAi} - + - + - +
n 10 16 10 14 10 10

I
peb-Gal4
Or83c lbe Merge
Or23a lbe Merge
peb-Gal4
Or83c lbl Merge
Or23a lbl Merge

J
peb-Gal4>UAS-Dcr-2
peb-Gal4>UAS-Dcr-2, UAS-lbe^{RNAi}
Or83c Or83c
Or23a Or23a
peb-Gal4>UAS-Dcr-2, UAS-lbl^{RNAi}
peb-Gal4>UAS-Dcr-2, UAS-lbe^{RNAi},-lbl^{RNAi}
Or83c Or83c
Or23a Or23a

K
No. of neurons
Or23a ** *** *** Or83c * *** *** Or43a ns
peb-Gal4> UAS-Dcr-2 + + + + + + + + + +
UAS-lbl^{RNAi} - + - + - + - + - +
UAS-lbe^{RNAi} - - + + - - + + - +
n 10 13 10 10 10 10 10 10 10 10

Mermet Figure 4

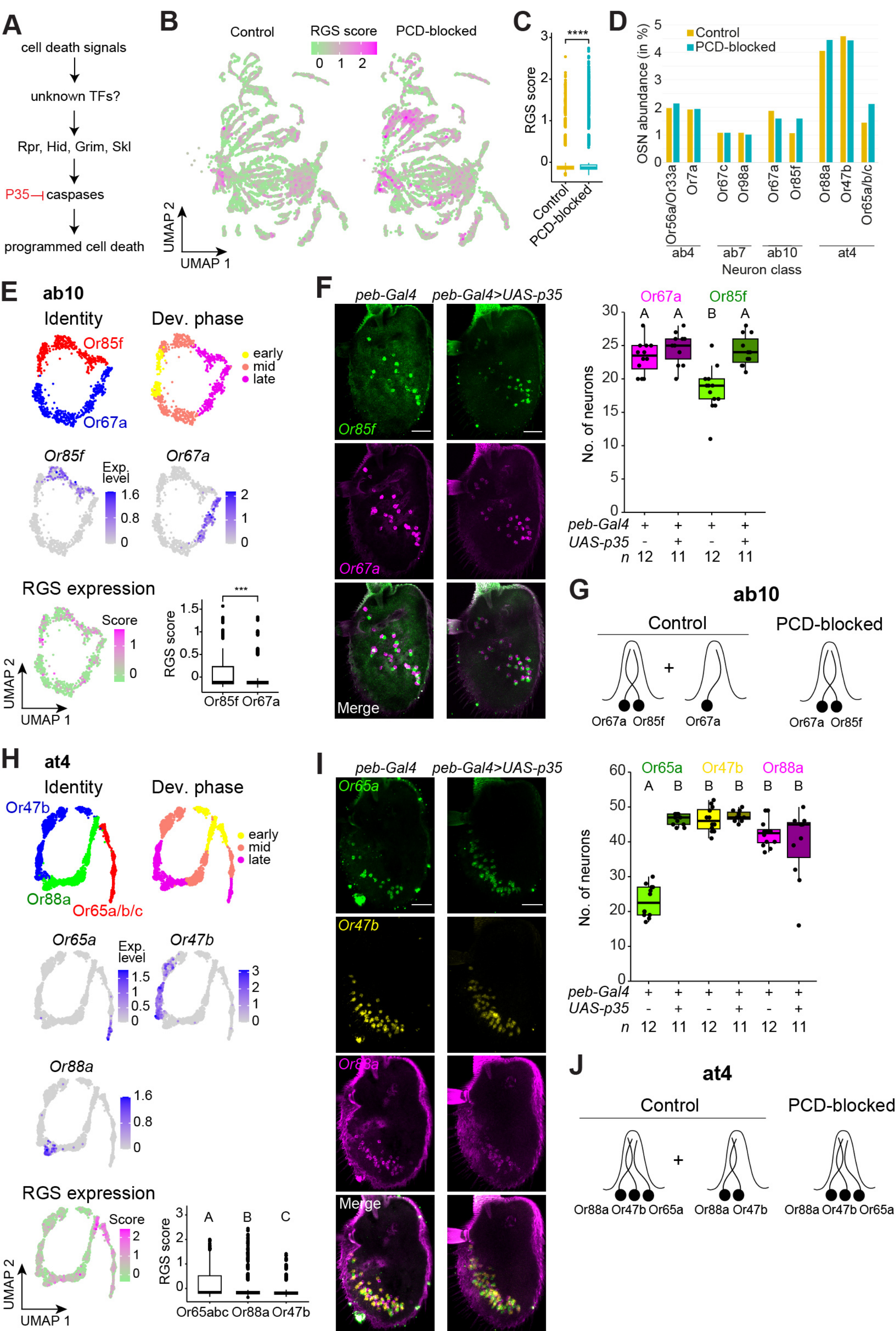

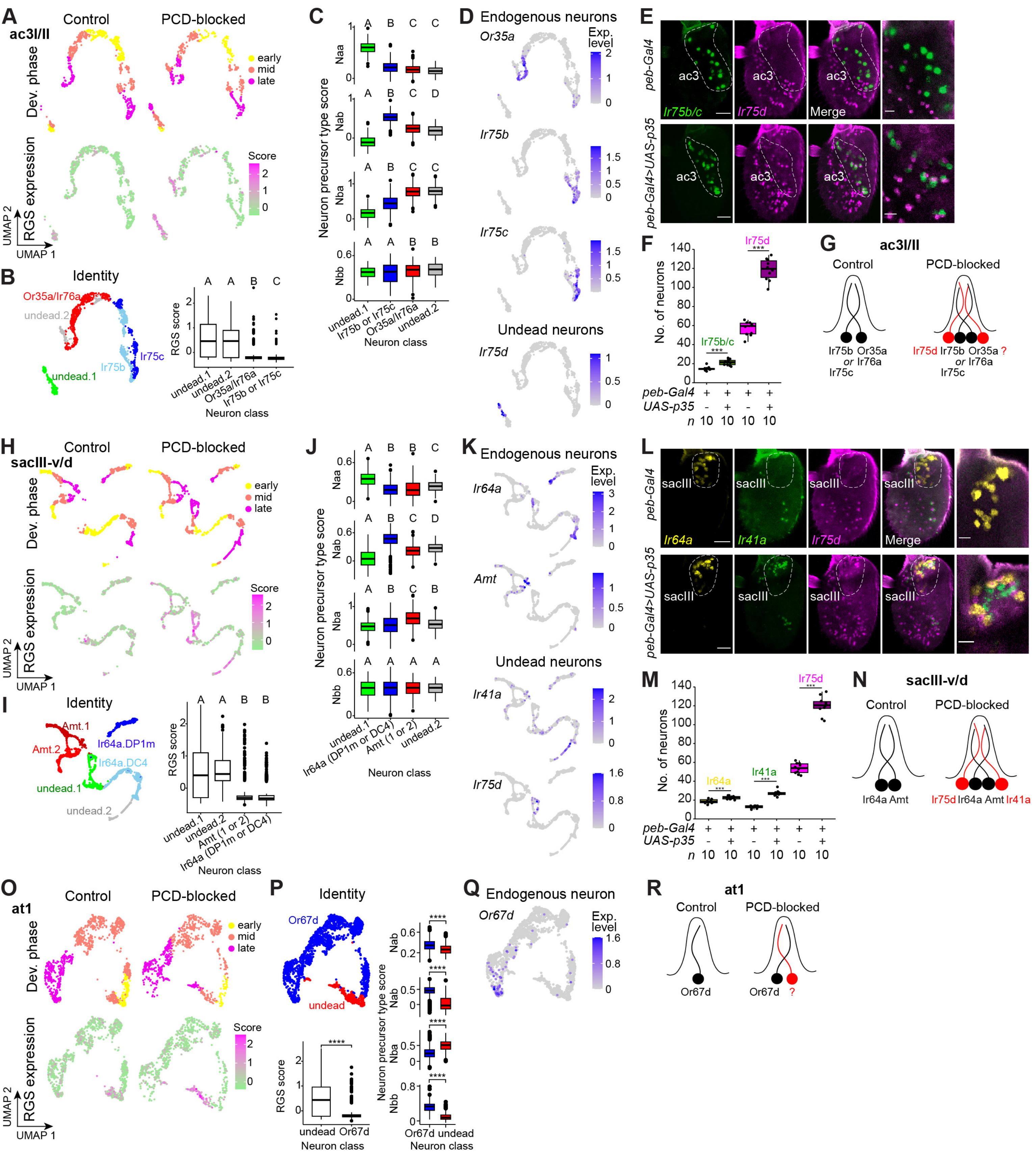

A
ac3I/II
Control
PCD-blocked
Dev. phase
early
mid
late
RGS expression
Score
UMAP 2
UMAP 1
B
Identity
Or35a/Ir76a
undead.2
undead.1
Ir75b
Ir75c
RGS score
Neuron class
C
Neuron precursor type score
Naa
Nab
Nba
Nbb
Neuron class
D
Endogenous neurons
Or35a
Ir75b
Ir75c
Exp. level
Undead neurons
Ir75d
E
peb-Gal4
peb-Gal4>UAS-p35
ac3
Ir75b/c
Ir75d
Merge
F
No. of neurons
peb-Gal4
UAS-p35
n
G
ac3I/II
Control
PCD-blocked
Ir75b Or35a or Ir76a Ir75c
Ir75d Ir75b Or35a ? or Ir76a Ir75c
H
sacIII-v/d
I
Amt.1
Amt.2
Ir64a.DP1m
Ir64a.DC4
J
K
Ir64a
Amt
Ir41a
L
sacIII
Ir64a
Ir41a
M
N
sacIII-v/d
Ir64a Amt
Ir75d Ir64a Amt Ir41a
O
at1
P
Or67d
undead
Q
Endogenous neuron
Or67d
R
at1

Mermet Figure 6

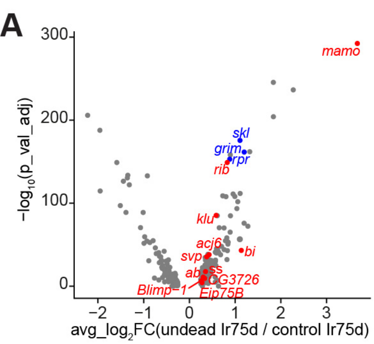

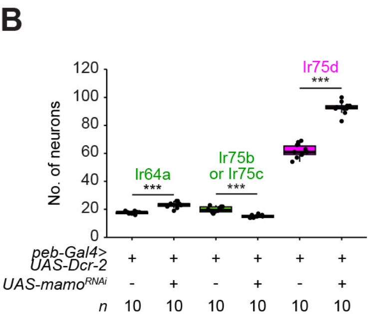

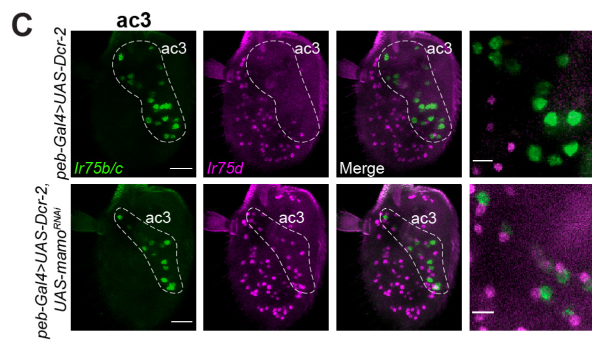

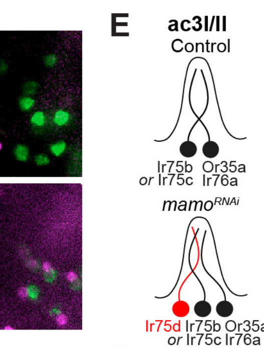

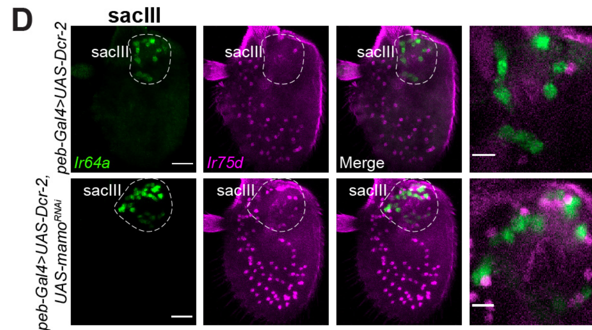

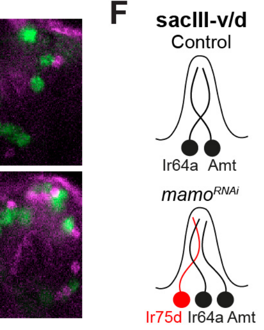

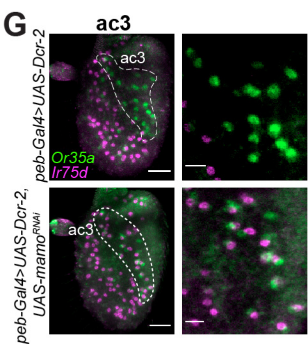

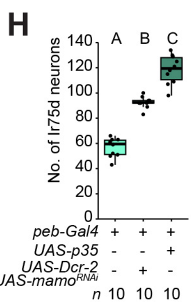

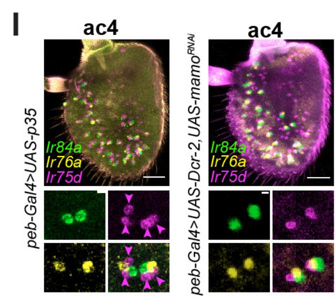

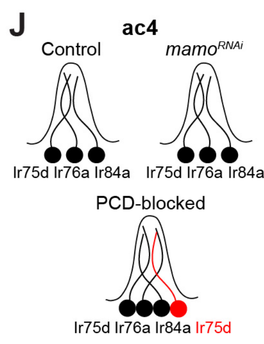

Mermet Figure 7

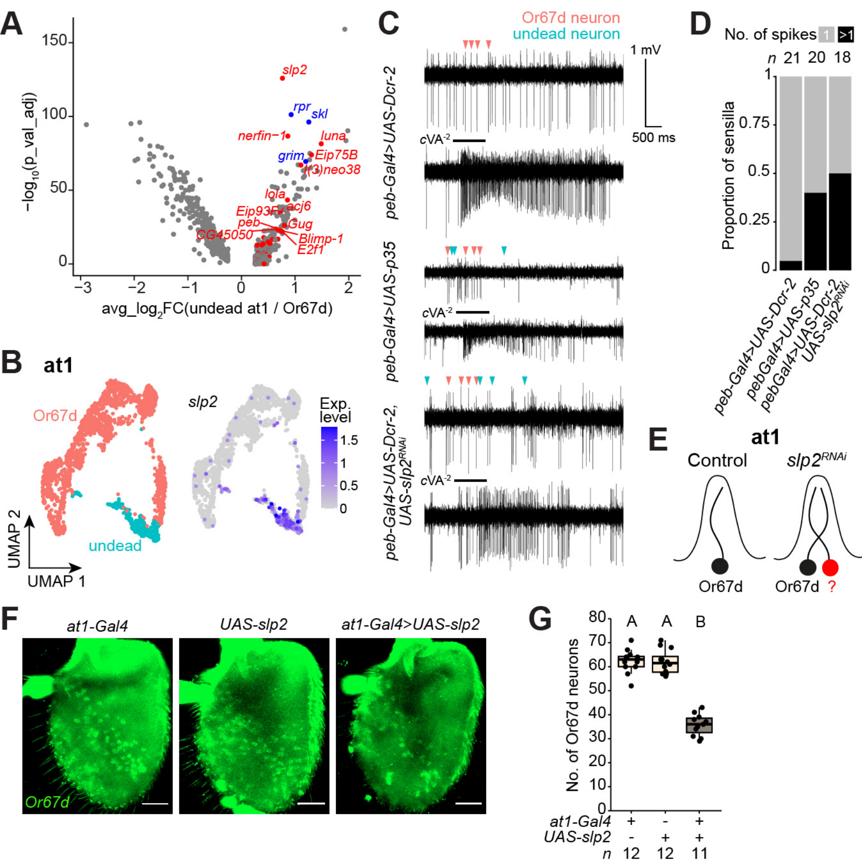

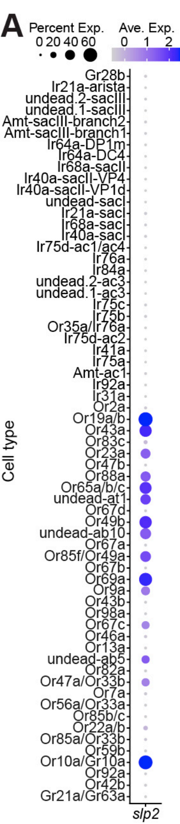
A
Percent Exp.
0 20 40 60
Ave. Exp.
0 1 2
Gr28b
Ir21a-arista
undead.2-sacIII
undead.1-sacIII
Amt-sacIII-branch2
Amt-sacIII-branch1
Ir64a-DP1m
Ir64a-DC4
Ir68a-sacII
Ir40a-sacII-VP4
Ir40a-sacII-VP1d
undead-sacI
Ir21a-sacI
Ir68a-sacI
Ir40a-sacI
Ir75d-ac1/ac4
Ir76a
Ir84a
undead.2-ac3
undead.1-ac3
Ir75c
Ir75b
Or35a/Ir76a
Ir75d-ac2
Ir41a
Ir75a
Amt-ac1
Ir92a
Ir31a
Or2a
Or19a/b
Or43a
Or83c
Or23a
Or47b
Or88a
Or65a/b/c
undead-at1
Or67d
Or49b
undead-ab10
Or67a
Or85f/Or49a
Or67b
Or69a
Or9a
Or43b
Or98a
Or67c
Or46a
Or13a
undead-ab5
Or82a
Or47a/Or33b
Or7a
Or56a/Or33a
Or85b/c
Or22a/b
Or85a/Or33b
Or59b
Or10a/Gr10a
Or92a
Or42b
Gr21a/Gr63a
Cell type
slp2

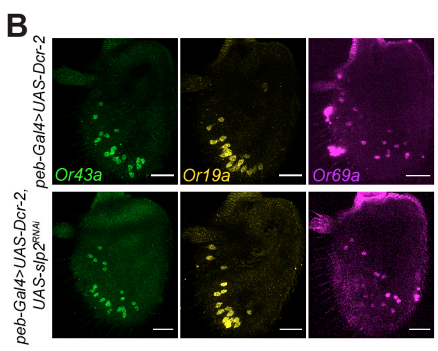
B
peb-Gal4>UAS-Dcr-2
Or43a
Or19a
Or69a

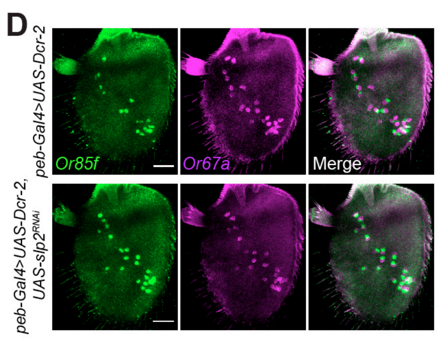
peb-Gal4>UAS-Dcr-2, UAS-slp2RNAi

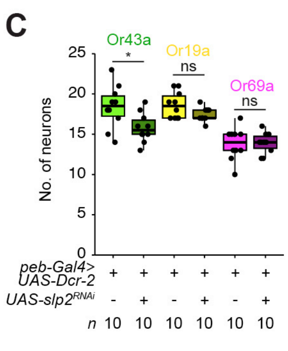
C
Or43a
Or19a
Or69a
*
ns
ns
No. of neurons
25
20
15
10
5
0
peb-Gal4> UAS-Dcr-2
UAS-slp2RNAi
n 10 10 10 10 10 10

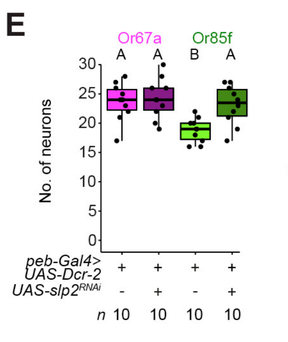
D
peb-Gal4>UAS-Dcr-2
peb-Gal4>UAS-Dcr-2, UAS-slp2RNAi
Or85f
Or67a
Merge
E
Or67a
Or85f
A A B A
No. of neurons
30
25
20
15
10
5
0
peb-Gal4> UAS-Dcr-2
UAS-slp2RNAi
n 10 10 10 10

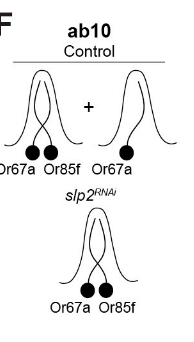
F
ab10
Control
+
Or67a Or85f Or67a
slp2RNAi
Or67a Or85f

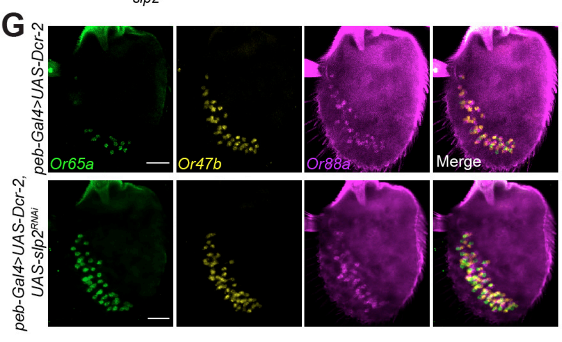
G
peb-Gal4>UAS-Dcr-2
peb-Gal4>UAS-Dcr-2, UAS-slp2RNAi
Or65a
Or47b
Or88a
Merge

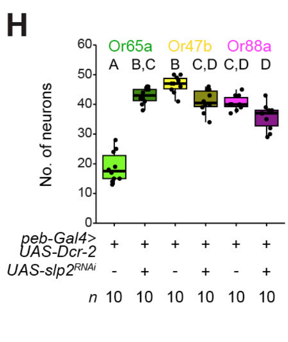
H
Or65a
Or47b
Or88a
A B,C B C,D C,D D
No. of neurons
60
50
40
30
20
10
0
peb-Gal4> UAS-Dcr-2
UAS-slp2RNAi
n 10 10 10 10 10 10

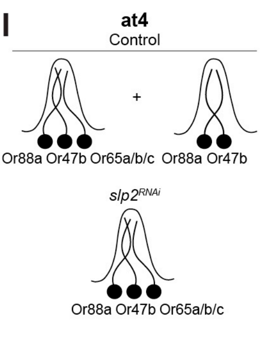
I
at4
Control
+
Or88a Or47b Or65a/b/c Or88a Or47b
slp2RNAi
Or88a Or47b Or65a/b/c

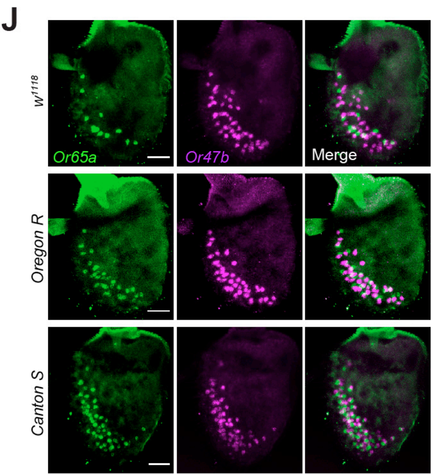
J
w1118
Oregon R
Canton S
Or65a
Or47b
Merge

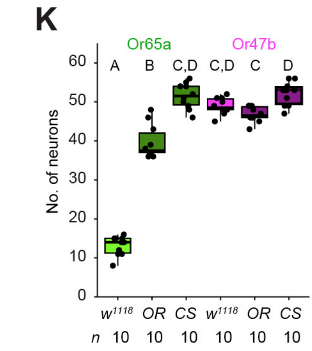
K
Or65a
Or47b
A B C,D C,D C D
No. of neurons
60
50
40
30
20
10
0
w1118 OR CS w1118 OR CS
n 10 10 10 10 10 10

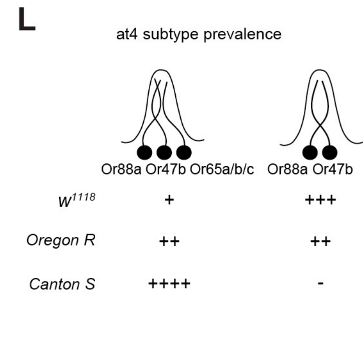
L
at4 subtype prevalence
Or88a Or47b Or65a/b/c
Or88a Or47b
w1118 + +++
Oregon R ++ ++
Canton S ++++ -